INFORMATION TO USERS

This material was produced from a microfilm copy of the original document. While the most advanced technological means to photograph and reproduce this document have been used, the quality is heavily dependent upon the quality of the original submitted.

The following explanation of techniques is provided to help you understand markings or patterns which may appear on this reproduction.

1. The sign or "target" for pages apparently lacking from the document photographed is "Missing Page(s)". If it was possible to obtain the missing page(s) or section, they are spliced into the film along with adjacent pages. This may have necessitated cutting thru an image and duplicating adjacent pages to insure you complete continuity.

2. When an image on the film is obliterated with a large round black mark, it is an indication that the photographer suspected that the copy may have moved during exposure and thus cause a blurred image. You will find a good image of the page in the adjacent frame.

3. When a map, drawing or chart, etc., was part of the material being photographed the photographer followed a definite method in "sectioning" the material. It is customary to begin photoing at the upper left hand corner of a large sheet and to continue photoing from left to right in equal sections with a small overlap. If necessary, sectioning is continued again – beginning below the first row and continuing on until complete.

4. The majority of users indicate that the textual content is of greatest value, however, a somewhat higher quality reproduction could be made from "photographs" if essential to the understanding of the dissertation. Silver prints of "photographs" may be ordered at additional charge by writing the Order Department, giving the catalog number, title, author and specific pages you wish reproduced.

5. PLEASE NOTE: Some pages may have indistinct print. Filmed as received.

University Microfilms International
300 North Zeeb Road
Ann Arbor, Michigan 48106 USA
St. John's Road, Tyler's Green
High Wycombe, Bucks, England HP10 8HR

SPIRAL-LIKE AURORAL FORMS: OBSERVATIONS AND A PROPOSED THEORY

A

DISSERTATION

Presented to the Faculty of the

University of Alaska in Partial Fulfillment

of the Requirements

of the Degree of

DOCTOR OF PHILOSOPHY

by

Thomas J. Hallinan, M.S.

Fairbanks, Alaska

May 1976

SPIRAL-LIKE AURORAL FORMS: OBSERVATIONS AND A

PROPOSED THEORY

RECOMMENDED:

John S. Murray

Joseph R. Kan

David W. Swift

Eugene M. Wescott

T. Neil Davis

Chairman, Advisory Committee

APPROVED:

K. B. McCutcheon

Director, Geophysical Institute

Apr. 16 1976

Date

C. Lee

Vice President for Research

22 Apr. 76

Date

SPIRAL-LIKE AURORAL FORMS: OBSERVATIONS AND A PROPOSED THEORY

Thomas J. Hallinan, M.S.
University of Alaska
Fairbanks, Alaska

ABSTRACT

An analysis of auroral images obtained from all-sky cameras, TV cameras, and satellite scanners shows that discrete arcs are typically subject to rotational distortions similar to those which occur in sheared layers of fluids. According to their spacing along the arc, their shapes, and their temporal behavior, these distortions are divided into three types: 1) Spirals are clockwise, vortex-like forms (viewed anti-parallel to $\vec{B}$), which are reversible and have spacings from 50 km to greater than 1,000 km; 2) Folds are reversible and sine-wave-like with a wavelength near 20 km. The sine wave has a pronounced skew in a clockwise sense; 3) Curls are irreversible counterclockwise vortices which have a typical spacing of 5 km. It is shown theoretically that, given sufficient path length and current density, the equilibrium configuration of an upward Birkeland current sheet must include clockwise spirals (or in some cases, folds) at its free end. The spatial growth rate of these spirals is given by a modified form of the Kelvin-Helmholtz dispersion relation. Counterclockwise curls have been shown theoretically and experimentally to occur in negative charge sheets. The sudden formation of a negative charge sheet coincident with the upward current sheet corresponds to the formation of a V-shaped double layer. The current densities required for spirals, folds, or double layer formations are all of order 10^{-5} amp/m^2, in agreement with experimental values determined in the evening and midnight sectors of the auroral zone.

ACKNOWLEDGEMENTS

The research reported in this thesis was carried out under the guidance of an advisory committee consisting of Dr. T. Neil Davis (Chairman), Dr. Joseph R. Kan, Dr. John S. Murray, Mr. Daniel W. Swift and Dr. Eugene M. Wescott. In addition, much advice and support was provided by other members of the staff at the Geophysical Institute, University of Alaska. In particular, I acknowledge the help provided by Dr. Syun I. Akasofu (who suggested the thesis topic), Dr. Gerald J. Romick, Dr. Ola Røyrvik, Dr. Charles S. Deehr, and Mr. Hans C. Stanbaek-Nielsen. I also received valuable encouragement from Dr. Harold F. Webster (General Electric Corporation Research and Development Center) and from Dr. Lewis Linson (Avco Everett Research Laboratory).

Mr. Garry F. Meltvedt, Mr. Larry R. Sweet and Mr. Russell F. Beach were responsible for much of the data acquisition. I am especially grateful to Miss Judith T. Holland who typed the manuscript and provided assistance wherever possible. Finally, I wish to pay tribute to the memory of Dr. Carl Gartlein who first inspired my interest in the aurora.

The aurora imagery data from U. S. Air Force satellites were made available by the Air Weather Service through the National Geophysical and Solar-Terrestrial Data Center, EDS, NOAA, Boulder, Colorado. The research reported in the thesis was supported primarily by the Atmospheric Sciences Section, National Science Foundation Grant GA-28079 and by the National Aeronautics and Space Administration Contract NGR 02-001-087.

TABLE OF CONTENTS

LIST OF ILLUSTRATIONS

The small arrows indicate the direction of the x-y component of the magnetic field. Note the points of accumulation at $y = a$, $x = \frac{3\pi}{4}$ and at $y = -a$, $x = \frac{\pi}{4}$.

Figure 13 In the linear analysis the current sheet distortion consists of sine waves on the two boundaries. The phase angle (Kx_o) between the two surface waves in Fig. 2 is 0.35π and the wavelength to thickness ratio ($\lambda/2a$) is 7.9. These values correspond to the fastest growing mode. There is an accumulation of field lines and of current in the regions near x_1 and x_2. The distortion of the current sheet is clockwise with respect to these values of x.

Figure 14 In Fig. 14, the quantity $i\beta B_o/\mu_o j_o$, which is proportional to the growth rate, is plotted as a function of the dimensionless number Ka. The wavelength to thickness ratio ($\lambda/2a$) is shown as a separate scale. The quantity Kx_o/π, which is a measure of the phase angle between the two surface distortions, is also plotted. The largest growth occurs for $Kx_o = 0.35\pi$ and $\lambda/2a = 7.9$. This leads to spirals. Larger values of $\lambda/2a$ correspond to smaller phase angles and hence result in folds.

Figure 15 This figure is a schematic illustration of the development of a spiral array. An initial local current enhancement ($x = 0$ in part a) results in a fold (b) and further enhancement and distortion in (c). In (d) a spiral has formed and a new ripple is beginning to appear some distance (λ) to the right of the initial disturbance.

Figure 16 (After Homann, 1936) Streak lines in the wake behind a circular cylinder in a stream of oil illustrate the form which should be assumed by a balanced pair of oppositely-directed Birkeland sheet currents.

LIST OF TABLES

CHAPTER 1

INTRODUCTION

A full understanding of the magnetospheric processes which produce the aurora must include a knowledge of the magnetic and electric fields in and near the aurora. In the last several years, great progress has been made in measuring these fields. They have been measured *in situ* with rocket- and satellite-borne sensors (Gurnett and Frank, 1973; Heppner, 1972; Zmuda and Armstrong, 1974; Sugiura, 1975; Anderson and Cloutier, 1975) and from the ground with shaped charges of barium which paint individual magnetic field lines (Wescott et al., 1975a). The electric fields have also been measured with incoherent scatter radar (Doupnik et al., 1972), barium thermite releases (Wescott et al., 1969; Davis and Wallis, 1972), balloons (Mozer and Serlin, 1969), and doppler shifts of optical emissions from ambient ions (Hays and Roble, 1971).

As a result of this progress in measurement techniques, there is an increasing understanding of the distribution of the magnetospheric convection electric field and of the magnetospheric and ionospheric current systems. However, for a variety of reasons, it is usually difficult to accurately associate the measured fields with specific auroral forms. This difficulty is particularly true of the magnetic field measurements. At present, there are probably less than a dozen determinations of the Birkeland (field-aligned) currents within or near individual auroral arcs. The number of determinations of electric fields within or near auroras is far greater. However, all but a handful of these measurements have been made at altitudes below 1,000 km. Swift et al. (1975) offered many cogent reasons for believing that these electric fields are not always representative of the fields at higher

altitudes, i.e., the earth's magnetic field lines are not always equipotentials.

Consequently, despite the increased understanding of the global field patterns, a detailed knowledge of the time-dependent electric fields and Birkeland currents within discrete auroras is still lacking. In order to fill this gap in the knowledge of auroral substorm dynamics, a technique is needed for determining the electric field and the Birkeland current at many points simultaneously. Points within or near discrete auroral arcs are of particular interest.

Since the precipitating auroral particles are themselves guided by the ambient fields, a knowledge of auroral shapes and motions, cautiously interpreted, can add to our understanding of these fields. Rotational distortions and motions are especially worthy of study since their complexity is sufficient to distinguish between possible competing mechanisms, but not so great as to preclude analysis. Various workers have suggested that one or another of the rotational distortions might result from perpendicular electric fields (Alfvén, 1950; Webster, 1957; Gartlein, 1959; Kern and Vestine, 1961; Akasofu and Kimball, 1964; Hallinan and Davis, 1970) or from Birkeland currents (Hasegawa, 1970; Hallinan et al., 1972; Webster and Hallinan, 1973).

The purpose of this thesis is to provide a comprehensive understanding of the roles of electric fields and of field-aligned currents in producing observed rotational distortions in auroral arcs. In Chapter 2, the morphologies of the various rotational distortions are described. The material in Chapter 2 draws, to some extent, on earlier work (Hallinan, 1970; Hallinan and Davis, 1970) on small-scale rotational features and it extends the analysis techniques to large-scale distortions. It is shown

that there are three related but distinct rotational forms which regularly recur and that each of these forms results from some type of shear. At least two types of shear are required in order to explain the observations.

Chapter 3 describes the mathematics of vorticity (shear) as applied to auroral arcs. In a review of the experimental and mathematical basis for the charge sheet instability, it is shown that a sheet of charge, aligned parallel to a magnetic field, is unstable and forms a series of vortices referred to in fluid dynamics as a vortex street. The rotational sense of the vortices, which depends on the sign of the charge, indicates that auroral curls originate in a negative charge sheet. The dispersion relation, giving the vortex growth rate as a function of wavelength and of sheet thickness, is identical to the dispersion relation developed by Lord Rayleigh for the Kelvin-Helmholtz instability which occurs in sheared fluids.

In earlier work by this author (Hallinan et al., 1972) it was inferred intuitively that there should be a magnetic analog to the charge sheet instability. If there is a sheet of field-aligned (Birkeland) current, there is a component of the magnetic field which is oppositely directed on the two sides of the sheet. This reversal of the magnetic field is in a sense analogous to fluid shear; and if the analogy is valid, an upward-directed current sheet should produce spirals such as those observed in the aurora.

In the mathematical development of Chapter 3, it is shown that this analogy is in fact correct. The main difference is that, while the charge sheet is inherently unstable, the current sheet is stable in the sense that the spiral development occurs as a function of distance parallel to the magnetic field rather than as a function of time. The

magnetic field lines are analogous to fluid stream lines while electric current is analogous to fluid vorticity. The expression obtained for the growth rate is directly analogous to the Kelvin-Helmholtz dispersion relation.

An analysis of the geometrical distortions and of the resultant perturbation magnetic fields shows that the degree of symmetry is related to the wavelength. If the ratio of the wavelength to the thickness of the current sheet is large, the disturbances on the two sides of the sheet are nearly in phase. It is also shown that field lines accummulate along the surface of the current sheet at certain points. The rotational sense of the distortion, with respect to these points of accummulation, is determined by the direction of the current.

In Chapter 4 the various parts of the analysis are organized in a proposed model for the morphology of an auroral arc. In this model the current sheet and the charge sheet are related to each other through a discussion of V-shaped double layers as proposed by Swift et al., (1975) and by Block (1975).

After a discussion of the physical reasonableness of the underlying assumptions, the model is compared, qualitatively, to the observations described in Chapter 2. Finally, the equations developed in Chapter 3 are used to calculate the magnitudes and directions of typical Birkeland currents and electric fields, the calculated values then being compared with measured values.

CHAPTER 2

MORPHOLOGY

2.1 Introduction

Hallinan and Davis (1970) identified three distinct types of rotational distortions which regularly occur in auroral arcs. These three forms (curls, folds, and spirals) are illustrated in Fig. 1 as they appear when viewed antiparallel to the earth's magnetic field. The curls are counterclockwise vortices with a typical spacing (λ) of 5 km. The folds are sine waves which are skewed in a clockwise direction. They have a typical wavelength of 20 km. The spirals are clockwise vortices with a spacing of anywhere from 50 km to greater than 1,000 km. The major features of these types are summarized in Table 1.

TABLE 1

	Curls	Folds	Spirals
Rotational Sense	CCW	CW	CW
Reversible	No	Yes	Yes
Typical Wavelength	5 km	20 km	>50 km
Typical Lifetime	1 sec	10 sec	10 min

2.2 Instrumentation

In order to study the characteristics of these forms and their inter-relationships, a study of auroral images was undertaken. Dimensions relevant to the descriptions range from a few hundred meters to thousands of kilometers while time scales range from less than a second to tens of minutes or longer. Hence no data set obtained with a single instrument is adequate. The description of rotational forms is based on the analysis of auroral images obtained with three types of detectors

including ground-based, airborne, and satellite observations; Since the detectors were sometimes used with differing fields of view and exposure programs, there are six basic data sets.

1) Narrow-Field TV: Ultra-sensitive image orthicon television cameras combined with video tape recorders record the aurora at the rate of 60 fields per second. When used with a lens having a 105 mm focal length, the image orthicon TV camera has a field of view of 12^{o} x 16^{o}. Since the narrow-field TV data used in this thesis all pertain to auroras in or near the magnetic zenith, the distance to the aurora is ∿108 km (Störmer, 1955) and the field of view corresponds approximately to a horizontal rectangle 23 km x 30 km at the base of the auroras. The smallest horizontal resolution element is ∿70 m, but only for that part of the aurora located precisely on the field line which passes through the observation site (i.e., the form is in the magnetic zenith). The actual resolution is a function both of the distance of the form from the magnetic zenith and of the vertical extent of the form (Maggs and Davis, 1968), but is typically of order 200 m for the specific data used in this thesis.

The TV system responds to wavelengths between 4000 Å and 8000 Å. Because there are fast motions in the aurora, the prominent atomic oxygen line at 5577 Å, which has a lifetime of 0.75 sec, causes blurring of the auroral forms. In order to avoid this problem, some of the TV data were obtained through a broad-band red filter. The still longer lifetime 6300 Å atomic oxygen line has little effect on the images except to add to the background glow.

2) Medium-Field TV: In some cases the same TV cameras discussed above were used with 35 mm focal length lenses providing a field of view

36^{o} x 48^{o} corresponding to a 61 km x 91 km rectangle at the assumed auroral lower border height of 105 km. The limiting resolution is ∿200 m near the center of the picture, but is substantially poorer near the corners because of the large distance from the magnetic zenith.

The spectral and temporal characteristics are the same as those of the narrow-field TV system.

3) Wide-Angle TV Camera: A "fish-eye" type of optical system was used with the TV cameras to provide a circular field of view of ∿140^{o}. This field of view corresponds to a circle of ∿560 km diameter at auroral altitude. The horizontal resolution near the center is of order 1 km and degrades toward the edges. The spectral and temporal characteristics are the same as those of the narrow-field TV system.

4) 16 mm All-Sky Cameras: By using a system of mirrors along with a conventional lens, an image, with a circular field of view of 180^{o}, is formed on 16 mm film. The 16 mm all-sky images used here were obtained at the rate of one per minute with exposure times of ∿15 seconds. The field of view corresponds to a circle of ∿2,000-km diameter at 100 km altitude, but there is considerable distortion near the edges. The resolution, of order 1 km near the center, is very poor near the edges. Rapidly moving forms are sometimes blurred beyond recognition by the long exposure time.

5) 35 mm All-Sky Camera: A "fish-eye" lens is used to image a 165^{o} circle onto 35 mm film. The field of view is ∿1,160 km at auroral altitude. The images used in this thesis were obtained at the rate of 12 per minute and with 3-second exposures. Because of the shorter exposure time and higher repetition rate, these data are more suitable than the 16 mm all-sky data for studying the dynamical aspects of the aurora.

6) DMSP Satellite Images: Since 1973, the U.S. Air Force has made available to the scientific community images obtained from its meteorological satellites. These satellites are in ∿850 km altitude polar orbits. They form the images by scanning the scene with a rotating mirror while the satellite motion provides a scan along the satellite ground track. The mirror sequentially reflects the various points in the scene onto an optical sensor which converts the light intensity into an electronic signal. This signal is transmitted to the ground where it is reconstructed into a complete optical image which is recorded on film.

The resultant images have a resolution of ∿3 km at the subsatellite point and poorer resolution elsewhere. The cross-track scan width is ∿2,960 km (Snyder et al., 1974). Many passes produce images of the entire nighttime portion of the auroral oval. The repetition rate (orbital period) is ∿102 min, and the scanning of the auroral zone takes approximately 15 min. The spectral response is 4,000 Å to 11,000 Å, peaking near 9,000 Å.

These images are particularly useful for examining large forms such as spirals. However, they convey no information concerning the dynamics of auroral forms. The 15-min scan period can distort the shapes of rapidly moving forms.

2.3 Data Selection

The specific data selected for analysis include the following:

January 1958 - College, Alaska and Barrow, Alaska all-sky photographs (one frame per minute).

March-April 1968 - Aircraft conjugate flights over Alaska and conjugate paths in the Southern Hemisphere. All-sky photographs

(12 exposures per minute). Narrow-field television (60 fields per second).

November 1967 - Aircraft flights over NWT, Canada. All-sky photographs (12 exposures per minute). Narrow-field television (60 fields per second).

1972-1973 - DMSP satellite No. 6530 images of both hemispheres; one image per hemisphere each 102 minutes.

1973-1974 - College, Alaska wide-angle (140^{0}) television recordings (60 fields per second).

In addition to these specific data sets, ten years of auroral TV observations serve as background in developing the qualitative descriptions.

2.4 Conventions and Definitions

Before proceeding with the description of rotational forms, it is useful to establish some conventions to be followed throughout the thesis.

1) Rotational motions are designated as clockwise or counterclockwise as they would appear to an observer viewing in a direction antiparallel to the magnetic field ($\vec{B}$). This is equivalent to looking up at the aurora in the Northern Hemisphere or looking down at the aurora in the Southern Hemisphere.

2) Rotational shapes are designated by the sense of rotation which would be necessary to distort an arc into the observed shape. This convention is followed whether or not actual rotational motions are observed.

3) All velocities and all distances perpendicular to $\vec{B}$ refer to the base of the visible aurora which is assumed to be near an altitude of 100 km.

4) All values of the perpendicular electric field and of the Birkeland current are referenced to the 100-km level even though it is recognized that, in some cases, measurements obtained at higher altitudes may not simply map down to the 100-km level.

5) A vortex street is defined, as in fluid dynamics, as an array of vortices strung out with quasi-periodic spacing along an arc.

6) All latitudes listed are invariant latitude.

7) Universal dates and times are used throughout except where otherwise noted.

2.5 Arcs - The Basic Discrete Auroral Form

The simplest and most common auroral forms are discrete arcs. These relatively thin forms often stretch hundreds and even thousands of kilometers roughly parallel to the statistical auroral oval. In the polar cap they tend to be aligned parallel to the earth-sun direction (Davis, 1962). It has been shown through the use of rocket-borne particle detectors that each arc is the ionospheric end of a sheet of precipitating particles (primarily electrons) which extends out an unknown distance into the magnetosphere (Johnstone, 1974; Boyd, 1973).

The thicknesses of auroral arcs, as determined from all-sky images, are of order 10 km (Kim and Volkman, 1963). However, these arcs are usually composed of several smaller, roughly parallel arc-like features which can be seen in the high resolution TV images. Maggs and Davis (1968) determined that the thicknesses of these smaller features, which they called arc elements, are of order 100 m. At the other end of the size scale are groupings of arcs or arc systems within which the arcs are roughly parallel and seem, in their motions and distortions, to act somewhat as a single unit. These systems have thicknesses of order

100 km (Maggs and Davis, 1968).

It is these arc elements, arcs and arc systems which become distorted to form the curls, folds, and spirals. Specifically, curls form only in the arc elements while spirals form both in the arcs and the arc systems. Folds can form both in arc elements and in arcs.

2.6 Rays, Curls, and Folds

One of the first signs of increasing auroral activity is the appearance of rays in the auroral arcs (Heppner, 1954; Akasofu and Kimball, 1964).

The rays can be stationary, but usually they move rapidly along the arc. When viewed from directly below, the rays are sometimes seen to be folds in the arc, but more often they are small vortex structures called curls (Hallinan and Davis, 1970). In general, the stationary rays are likely to be folds while the rapidly moving rays are usually curls. The curls have been described in some detail by Hallinan and Davis (1970). They are counterclockwise (viewed antiparallel to $\vec{B}$) vortex streets occurring in individual arc elements. They have a typical wavelength of 5 km and typical horizontal velocities of 0-20 km/sec. When they occur in two neighboring arc elements, they move in opposite directions such that the motions are always counterclockwise with respect to a point between the elements. In ten years of television observations, no exception has been noted either to the rotational sense of individual curls or to the convention for relative motions in neighboring arc elements.

At times, particularly in the morning sector, the rays are very tall and thin. Then the geometry precludes observation of their cross sections, so they cannot be positively identified as folds or curls.

Their relative motions, however, still follow the above convention.

The curls are a transient phenomenon, the lifetime of an individual curl being of order one second. They are irreversible in their formation (never unwind) and are never static, i.e., throughout the lifetime of a curl, it is rotating noticeably in a counterclockwise direction.

The folds, although less common than curls, are frequently observed. They appear as sine waves which are skewed in a clockwise fashion. They often occur in individual arc elements, but at times an entire arc is distorted into folds. Folds seem to occur especially often in the bounding elements of arcs. In these cases the motions of the folds, like those of curls, are invariably counterclockwise with respect to the center of the arc.

The rotational shape of the folds is unambiguously clockwise in all or most cases. The rotational motions, however, are confusing. The high-speed motions of individual irregularities within the folds, are counterclockwise (Oguti, 1974). In the 60-fields-per-second recordings obtained with television cameras, the counterclockwise motions appear to predominate. In all-sky films, which have a lower time resolution, the folds either suddenly appear already developed or they appear to evolve through clockwise motions. Unlike the curls, which are irreversible, the folds can "unwind" through counterclockwise motions.

The folds occur under conditions very similar to those that cause curls. In fact, it is quite common for the clockwise folds to change rather abruptly into counterclockwise curls.

2.7 Spirals

The description of the morphology of spirals is based on analysis

of DMSP and all-sky camera images.

2.7.1 Definition

Spirals are large clockwise vortex structures that can occur singly or as parts of spiral arrays similar in appearance to fluid vortex streets. They are qualitatively similar to curls, but are distinguished from the curls by their large size (one to two orders of magnitude larger than curls) and their slower time scales (lifetimes on the order of minutes or tens of minutes). They involve all the elements of an arc or arc system rather than occuring in individual arc elements. The rotational sense is opposite to that of curls.

2.7.2 Morphology and Occurrence of Auroral Spirals

Anger and Lui (1973) described a large spiral detected by the ISIS auroral scanner; this spiral had a diameter of 1,300 km, a size much too large to be included in the field of view of a ground-based all-sky camera. Other examples of spirals, selected from the DMSP topside scanner images are shown in Fig. 2. Examples with less symmetry, but which nevertheless exhibit spiral-like characteristics appear in Fig. 3. Spiral configurations are most easily recognized from below when centered near the observer's zenith, as in Fig. 4A. Large spirals or those not centered on the ground-based observers zenith (Fig. 4B, C, D) are more difficult to recognize.

Spirals evolve from arc-like auroras; during the evolution the formation may not be readily identified as being a spiral, or perhaps the evolution becomes arrested or distorted. Consequently it is not always obvious whether or not a particular convoluted auroral feature is actually a spiral. Once one recognizes the existence of the spiral configurations in the aurora, the person notices them frequently and

may tend to identify as spirals auroral convolutions caused by mechanisms other than that which causes spirals. Special effort has been made here to avoid this tendency when developing various statistical results pertaining to spirals.

The essential distinguishing features of spirals are shape, size and probably sense of rotation. The only other vortex configuration in the aurora is the curl; its diameter never exceeds a few kilometers, and its sense of rotation is always counterclockwise viewed antiparallel to $\vec{B}$.

2.7.3 Spiral Size

Previously reported measurements are contained in papers by Akasofu and Kimball (1964), ∿400 km; Akasofu et al. (1965a), ∿500 km; Akasofu et al. (1965b), ∿600 km; Akasofu et al. (1969), ∿400 km; Anger and Lui (1973), ∿1,300 km.

The distribution of diameters observed in the DMSP images is shown in Fig. 5 where, in each case, the minimum observed diameter is taken. The open-bar plot in Fig. 5 is compiled counting each spiral as one sample, the shaded-bar plot counts each spiral street as one sample wherein the street consists of one or more spirals and where the diameter represents the average of the minimum diameters of the spirals comprising the street.

In addition to the DMSP measurements, the diameters of eighteen spirals were measured from all-sky photographs. They ranged from 20 km to 600 km.

Since spirals are not observed with narrow-field TV cameras (FOV≈ 23 km x 30 km), the cutoff near 20 km should be considered real rather than being a result of the limited resolution in the DMSP and all-sky data.

The spirals typically are elongated in the direction of the street axis, i.e., in the approximate direction of local horizontal auroral alignment. Figure 6 contains a plot showing the distribution of the ratio of major to minor spiral diameters. The ratio varies up to 4 with a median value of 1.7.

2.7.4 Spiral Spacing

Single spirals occur, however they frequently appear in arrays (vortex streets) containing two or more spirals. In some instances, such as the one labelled Pass 403 in Fig. 2, the spirals within a street are identical in size and configuration; more frequently there is a monotonic variation in size along the street. It will be shown in Chapter 3 that the spacing between spirals is theoretically predictable; hence the observed spacing in auroras is of significance. Figure 7 shows the results of measurements from DMSP images of the spacing to diameter ratio (λ/D), where in each case the diameter is the average of minor axis diameters of two adjacent spirals. The median λ/D ratio is 5, and the diagram shows that most values of the ratio lie between 3 and 8. In the remarkably symmetrical example shown in Fig. 2 (Pass 403), the λ/D ratio is 3.0. Since it is predicted from theory, the ratio of the wavelength to arc width (2a) is perhaps of more value than the λ/D ratio. It is difficult to accurately measure the widths of the arc structures involved in the spiraling; however, the results of 18 such measurements show a median value for $\lambda/2a$ of 20 with the range from 13 to >30; more than half of the measurements fall in the range 17-23.

2.7.5 Spiral Location and Occurrence Within the Substorm

Spiral or spiral-like formations are seen in excess of 30% of the DMSP images. Spirals occur most frequently in the evening and

midnight sectors of the auroral oval during the expansion and early recovery phases of the auroral substorm. If a substorm expansive phase begins under relatively quiet conditions when the auroral oval is narrow and contracted, single spiral or spiral-like formations develop within the narrow oval near the midnight meridian. Examples are seen in DMSP passes 448 and 449 acquired December 10, 1972 (Akasofu, 1974, pp. 640-643). Under more active conditions, spirals develop along the oval in the sector extending from the midnight meridian westward to the dusk meridian or perhaps beyond. Then, the width of the oval expands and the spirals typically are most prevalent near the poleward boundary. The westward-traveling surges identified by Akasofu et al., (1965a) are spirals or spiral-like formations. During the late expansion or early recovery phases of the substorm, DMSP images frequently show bright auroral band systems that, in the midnight sector, are well poleward of the normal oval. In the evening sector, these seem to connect to a large spiral or spiral remnant in the oval. Spirals are common in these bands which may reach poleward as far as 85^{o} latitude in the midnight meridian. Spirals along these bands may be observed somewhat eastward of the midnight meridian. Examples are seen in DMSP passes 492, acquired December 13, 1972 (Akasofu, 1974, p. 703); 1094 and 1100, acquired January 25, 1973; passes 1110 and 1114, acquired January 26, 1973 (Snyder et al., 1974); and passes 815, 873, 882 and 911, acquired January 1-11, 1973 (Akasofu, 1974, pp. 656, 695, 700, 704).

The spiral configurations described above all appear to be associated with substorm expansion and early-recovery phases; they occur in the sector lying between 18 hours and 03 hours in the latitude range between the equatorward boundary of the aurora and approximately 85^{o}, as

shown on Fig. 8. Figure 8 is a schematic diagram showing the locations of spiral forms in local geomagnetic time and relative to the location of the equatorward boundary of the diffuse aurora. Numbers near each bar refer to DMSP satellite pass numbers; the bars are aligned along the major axis of the spirals, typically the direction of local auroral alignment. Latitudinal positions of the bars on Fig. 8 are only approximate since the data have been normalized to a particular equatorward boundary lying at 65^{o} latitude in the midnight meridian. Even so, the latitudinal positions are correct to within a few degrees in practically all cases.

The DMSP data show a second grouping of spirals lying in the dawn meridian (04 hours to 08 hours, local geomagnetic time) between the equatorward boundary of the diffuse aurora and latitude 82^{o}. Unlike the spirals in the evening and midnight sectors, the dawn spirals occur mostly during quiescent periods and are typically in weak, apparently quiet auroras. The major axes of these spirals and the alignment of the arc-like auroras within which they occur are aligned approximately in the sun-earth direction rather than parallel to the local auroral oval. The symmetric spiral street in Fig. 2 (pass 403) belongs to this group.

All-sky images occasionally show short-lived (<2 min), relatively small spirals in or near the auroral oval close to the dawn meridian. These occur under very active conditions. Due to the infrequent appearance and their transient nature, they have not been seen in the DMSP images.

While Fig. 8 shows schematically the locations of spirals, a different viewpoint is provided by Fig. 9. Here the occurrence frequency of spirals is plotted as a function of local time for two stations: Barrow, Alaska (Lat. 69^{o}) and College, Alaska (Lat. 65^{o}). The data base

consisted of 12 nights during the month of February, 1958. These 12 nights were the only nights during the month for which there is satisfactory cloud-free data available from both sites. The two stations approximately bracket the statistical auroral zone, and the two locations had ab ut the same auroral incidence during this time period (Davis, 1961).

Figure 9 shows that there are far more spirals in the evening than in the morning and that spirals are more common at Barrow than at College. The total number of spirals observed from Barrow is three times the number observed from College. Since the auroral incidence is similar at the two stations, it can be concluded from this observation alone that the spirals are generally near the poleward edge of the aurora.

2.7.6 Spiral Evolution

Akasofu and Kimball (1964) documented the development and decay of a spiral appearing over Point Barrow during the great auroral display of February 11, 1958. This spiral, approximately 500 km in diameter, wound up and then unwound over a period of 30 min. During the winding up, rotational speeds near 900 m/sec occured, and during the unwinding the speed was near 830 m/sec. In order to further examine rotational motions, the conjugate flight all-sky photographs, taken at the rate of 12 per minute, were used to measure the growth and decay of 15 spirals of average diameter 80 km. Development and decay times of these spirals ranged from 15 sec to 195 sec with an average of 65 sec to reach to or decay from a maximum of 3 revolutions.

In some cases, there is remarkable temporal symmetry such that, when the all-sky films are projected in cine fashion, it is difficult to tell whether the time is running forward or backward, i.e., clockwise

motions are followed by counterclockwise motions, no matter which way the film is projected. This reversibility is in marked contrast to curls. They are irreversible. When films of the curls are viewed in normal fashion, all motions are counterclockwise; when the film is reversed in time, all motions are clockwise.

Little information on the evolution of large spirals is available because of the difficulty of observing them from a single ground station and the low temporal resolution of satellite scanner data, i.e., one image per ∿100 min. Anger and Lui (1973) reported a large spiral that appeared on three successive ISIS passes. Viewing of DMSP data also gives the impression that once a large spiral has formed it may have enough persistence to be seen on the next pass 100 min later. In some cases the apparent persistance may be false, since there is no assurance that the same spiral is being observed on successive passes. The DMSP data also give the impression that the larger spirals often decay into broken, patchy auroral forms instead of unwinding back to arc-like aurora. It seems possible that the flute-like or torch-like serrated auroras seen extending poleward from the oval in the midnight and morning sectors during the substorm recovery phase (Snyder et al., 1974; Akasofu, 1974) are remnants of spirals.

2.7.7 Rotational Shape

Since data from both hemispheres are included, the convention used throughout this thesis is to always specify rotational motions and shapes as seen when viewed antiparallel to $\vec{B}$. This convention corresponds to looking up at the aurora in the Northern Hemisphere or looking down from above in the Southern Hemisphere. The rotational shape of the spiral is defined as the direction of rotation necessary

to follow the auroral arc from the spiral limb into the spiral center.

According to these definitions, each of the spirals observed in the DMSP data (∿150 examples) was clockwise. Of the 200 examples observed in the all-sky photographs, 189 were clockwise. None of the supposed counterclockwise spirals were satisfactory examples; it is likely that they were not actually spirals. It is concluded that all, or most, spirals are clockwise.

2.7.8 Occurrence of Curls and Folds Within Spirals

Hallinan and Davis (1970) reported that curls and folds occur typically in bright arcs during the breakup or during westward surges. But it is now clear that the breakups and surges usually are spirals. It thus appears statistically that counterclockwise curls occur within clockwise spirals. In order to check this behavior, the narrow field television recordings from the aircraft flights were examined for those periods during which the all-sky cameras showed overhead spirals. Figure 10 consists of three pairs of photographs, each pair including an all-sky photograph and a narrow-field TV image of a portion of the aurora in the all-sky image. Because of the differences in field of view and exposure time, the TV images look considerably different from the all-sky photographs. In each case, the narrow-field picture includes curls while the all-sky picture shows a spiral. In the more recent 140^{o} field of view TV images, it is possible on occasion to see the counterclockwise curls and clockwise folds within clockwise spirals.

2.7.9 Summary of Spiral Observations

Clockwise spirals, appearing singly or in spiral streets, are a common part of the active auroral display. They range in size from diameter 20 km to 1300 km. The spirals typically are elongated in

the direction of local auroral alignment. The median ratio of the major to minor axis is of 1.7; the ratio sometimes ranges as high as 4. When spirals occur in streets, the median ratio of the spacing λ to the average spiral diameter is 5, and the median value of the ratio of λ to the width of the auroral structure undergoing spiralling is 20.

Spirals occur in the evening and midnight sectors between the equatorward boundary of the aurora and geomagnetic latitude 85^{o} during the substorm expansion and early-recovery phase. These spirals develop relatively rapidly, in times ranging from a few tens of seconds to a few minutes. Some have been observed to unwind back to an arc-like configuration on the same time scale. There are indications that some of the larger of these spirals, once developed, persist for long periods and then decay in place to irregular or patchy auroral forms.

A second grouping of spirals, of apparently more quiescent nature, appears poleward of the dawn equatorward boundary of the auroral oval. Distinctive characteristics of these spirals are their occurrence in quiet phases of the display, their formation within linear auroras aligned in the sun-earth direction and their comparative weakness. The temporal resolution of the DMSP satellite scanner data in which these spirals are observed does not provide information on the time scales of their evolution.

The small scale structure within the clockwise spirals includes both clockwise folds and counterclockwise curls.

CHAPTER 3

MATHEMATICAL ANALYSIS

3.1 Introduction

The occurrence of vortex configurations in the aurora, on a small scale in curls and on a large scale in spirals, has a special significance: vortex configurations are common in nature whenever there is shear in a moving fluid; therefore vortices in the aurora imply shear. The observations of auroral motions confirm the presence of shear. There is an apparent velocity differential between the opposite sides of an arc element or of a multiple arc; this apparent velocity shear finds expression in the formation of vortices.

The presence of both clockwise and counterclockwise forms suggests that there are two types of shear in the aurora. Both types of shear seem intimately associated with the sheets of precipitating particles responsible for discrete auroral arcs. Since the curls and spirals are identical in appearance to fluid vortices, it is reasonable to seek, in association with precipitating sheets, vector field quantities which satisfy equations similar to those governing the velocity in an incompressible inviscid fluid. In a magnetic field, under the proper circumstances, there are two vector quantities which can each play a role similar to that of the velocity in an incompressible sheared fluid. These are the velocity of the frozen-in field lines in the presence of a divergent electric field (charge sheet) and the magnetic field itself in the presence of a field-aligned current. These two quantities are analyzed in the following sections.

3.2 Charge Sheet

The behavior of a sheet of charge in a magnetic field has been discussed by numerous authors. Cutler (1956) and Webster (1957) both demonstrated experimentally that a negatively charged sheet in a magnetic field develops into an array of counterclockwise vortices. A dispersion relation for the growth rate as a function of wavelength was derived, in the long wavelength limit, by Pierce (1956) and by Kyhl and Webster (1956). Derivations of a more general dispersion relation have been given by Gould (1960) and by Buneman et al. (1966).

The dispersion relation, (Eq. 5.5 from Buneman et al., 1966) is given in Eq. 1.

$$\omega = \frac{\omega_s}{2}\left[(1 - 2Ka)^2 - e^{-4Ka}\right]^{\frac{1}{2}} \tag{1}$$

where ω is the growth rate, 2a is the thickness of the charge sheet (see Fig. 11), K is the wave number ($K = 2\pi/\lambda$) along the charge sheet (x direction), and ω_s is the vorticity which is defined by:

$$\omega_s = \frac{\partial V_x}{\partial y} = \frac{1}{B_o}\frac{\partial E_y}{\partial y} = \frac{e}{B_o \varepsilon_o}(n_e - n_i) \tag{2}$$

e is the charge of an electron, and n_e and n_i are the electron and ion densities, respectively. B_o is the magnetic field strength. (The various symbols and their definitions are listed in Appendix I). Growth occurs (imaginary ω) for values of Ka between zero and 0.64.

It was observed by Buneman et al. (1966) that Eq. 1 is identical to the dispersion relation derived by Lord Rayleigh for the Kelvin-Helmholtz instability in fluid shear. Levy and Hockney (1968) and Joyce and Mont-

gomery (1973) have discussed the fact that space charge in a magnetic field is analogous to vorticity in a fluid. Following Levy and Hockney (1968), this analogy may be seen by taking the curl of the guiding center velocity perpendicular to the magnetic field.

$$\nabla \times \vec{V}_{\perp} = \nabla \times \frac{\vec{E} \times \vec{B}}{B^2} \tag{3}$$

Assuming that the magnetic field is straight and uniform (negligible current) and that the electric field is, at least approximately, independent of z, Eq. 3 may be rewritten as

$$\nabla \times \vec{V}_{\perp} = -\frac{\vec{B}_o}{B_o^2} \nabla \cdot \vec{E} = \frac{e}{B_o \varepsilon_o} (n_i - n_e) \hat{z} \tag{4}$$

The righthand side of Eq. 4 is the same as the vorticity defined in Eq. 2. Hence conservation of charge is equivalent to conservation of vorticity.

$$\frac{d}{dt} (\nabla \times \vec{V}_{\perp}) = 0 \tag{5}$$

Furthermore, the divergence of $\vec{V}_{\perp}$ is given by:

$$\nabla \cdot \vec{V}_{\perp} = \frac{1}{B^2} \nabla \cdot (\vec{E} \times \vec{B}) \tag{6}$$

$$\nabla \cdot \vec{V}_{\perp} = \frac{1}{B^2} \left[\vec{B} \cdot (\nabla \times \vec{E}) - \vec{E} \cdot (\nabla \times \vec{B}) \right] = 0 \tag{7}$$

In Eq. 7, both terms vanish due to the assumption of negligible current. Equations 5 and 7 (conservation of vorticity and incompressibility) are

the fundamental fluid equations from which the Kelvin-Helmholtz dispersion relation (Eq. 1) can be derived without further reference to electric or magnetic fields (see Appendix II).

Equation 1 is derived on the basis of the linearized equations of motion. Hence it contains no information concerning the shape that the charge sheet will assume as the instability becomes nonlinear. However, since Eqs. 5 and 7 are valid even in the nonlinear regime, it follows that the ultimate shape of a charge sheet in a magnetic field should be the same as that of a fluid shear layer. The charge sheet should form a vortex street. Levy and Hockney (1968) used a computer to perform a numerical analysis and confirmed that the charge sheet does indeed evolve into a row of vortices indistinguishable from those observed in fluid shear or those that Cutler and Webster had observed in their laboratory experiments with sheet electron beams. (In these experiments, the growth occurred as a function of distance rather than of time. In Appendix II it is shown that the dispersion relation appropriate to their experiments is the same as Eq. 1 provided that ω is regarded as the convective growth rate.)

In summary, it is now well understood that a sheet of charge in a magnetic field is unstable and will form a vortex street. If the charge excess is negative, the vortices will be counterclockwise. This result has been verified experimentally and in numerical calculations. It is intuitively reasonable in view of the correspondence between the equations governing guiding center drifts and those governing sheared fluids. A qualitative description of the physical mechanisms involved is provided by Webster and Hallinan (1973).

3.3 Current Sheet

It is clear from the morphology of vortex formations in the aurora that two vortex-forming mechanisms are required to explain both curls and spirals. There must be a field quantity, other than $\vec{E} \times \vec{B}$, that is in some sense analogous to a sheared fluid and which is closely related to the sheets of precipitating particles. If the aurora is coincident with a field-aligned (Birkeland) current sheet, these conditions are satisfied by the magnetic field.

The magnetic field is sheared in the sense that its horizontal component reverses from one side of the current sheet to the other. Since the auroral electrons follow the magnetic field, this shear should be reflected in their motions. It was on this basis that spirals were first associated with Birkeland currents (Hallinan et al., 1972; Webster and Hallinan, 1973).

In this thesis the linearized equations describing the equilibrium shape of a Birkeland current sheet are investigated. It is shown that the only equilibrium configuration, including perturbations, is one in which a disturbance grows exponentially with distance. The growth constant is given by an equation which is closely analogous to the Kelvin-Helmholtz dispersion relation for fluid shear.

It is also shown that the disturbance is inherently asymetric, the degree of asymetry depending on the wavelength. From an analysis of the long-wavelength limit, it is seen that there are specific points along the surfaces of the current sheet where field lines tend to accumulate. The local distortions are clockwise with respect to these points.

3.3.1 Development of Dispersion Relation for Spirals

In order to study magnetic shear, it is convenient to adopt

a simple model consisting of a single uniform sheet of field-aligned current in an otherwise straight and uniform magnetic field (Fig. 11). The ambient magnetic field B_o is in the z direction and the current sheet, initially in the x,z plane, is directed in the -z direction. In addition to the component of current along z, there is a small component along x which is necessary in order to maintain a force-free field configuration. Since the effect of the current is to change the angle of the field lines rather than to move whole flux tubes, it is reasonable to impose the boundary condition that, except for infinitesimal perturbations, the current sheet remain undistorted at one end (z = 0). Furthermore, since spirals are sometimes observed to be stable or even reversible, it is appropriate to look for equilibrium configurations of the current sheet that include variation along the z direction rather than seeking an instability as such. A further simplification, based on the observed quasi-periodicity of spirals along the arc, is to assume that the variation along x is periodic.

The magnetic field is assumed to consist of a zero-order field in the z direction consisting of the ambient field B_o and a small correction W due to current along x, a zero-order shear field in the x direction produced by the current sheet, and first-order perturbation fields. The magnetic field (webers/m^2) is then given by:

$$B_x = U + A_1 e^{i(Kx + \beta z)} \tag{8}$$

$$B_y = A_2 e^{i(Kx + \beta z)} \tag{9}$$

$$B_z = B_o + W + A_3 e^{i(Kx + \beta z)} \tag{10}$$

where the perturbation amplitudes A_1, A_2, and A_3 and the correction term W are as yet undetermined functions of y. The shear component of the magnetic field, represented by U, is given by:

$$U = \mu_o j_o y \qquad |y| \leq a \tag{11}$$

$$U = -\mu_o j_o a \qquad y < -a \tag{12}$$

$$U = \mu_o j_o a \qquad y > a \tag{13}$$

The current density j_o is in amp/m^2, and the current sheet thickness 2a is in meters.

Since an equilibrium field configuration is sought, the force is set equal to zero

$$\vec{j} \times \vec{B} = 0 \tag{14}$$

Equation 14 can be expanded to yield:

$$\frac{1}{\mu_o} (\vec{B} \cdot \nabla) \vec{B} - \frac{1}{2\mu_o} \nabla \vec{B}^2 = 0 \tag{15}$$

The application of Eq. 15 to the field equations 8-10, yields the following pair of equations

$$A_2 U' + i\beta (B_o + W) A_1 - iKA_3 (B_o + W) = 0 \tag{16}$$

$$\left[iA_2(KU+\beta B_o+\beta W)-(UA_1)'-B_oA_3'-(WA_3)'\right] e^{i(Kx+\beta z)} - UU' - (B_o+W)W' = 0 \quad (17)$$

The primes indicate differentiation with respect to y.

The other condition on $\vec{B}$ is Maxwell's law

$$\nabla \cdot \vec{B} = 0 \quad (18)$$

This yields a third equation

$$iKA_1 + A_2' + i\beta A_3 = 0 \quad (19)$$

The zero order solution to Eq. 17 is

$$W' = -\frac{UU'}{B_o+W} \approx -\frac{UU'}{B_o} \quad (20)$$

Equation 16 may be rewritten

$$A_3 = -\frac{i}{K(B_o+W)} A_2U' + \frac{\beta}{K} A_1 \quad (21)$$

In order to obtain a solution for A_2, use Eq. 21 to eliminate A_3 and A_3' from Eqs. 17 and 19.

Since distances parallel to B are large compared to distances along arcs, attention will be restricted to cases where $\beta << K$. Also $U << B_o$ and $W << B_o$. Hence terms including factors $\frac{\beta}{K}\frac{U}{B_o}$, $\frac{W}{B_o}$, or $\frac{\beta^2}{K^2}$ are eliminated. Equation 21 combined with Eq. 17 yields

$$iA_2 (KU + \beta B_o) - (UA_1)'$$

$$+ \frac{i}{K} (A_2'U' + A_2U'') - B_o \frac{\beta}{K} A_1' = 0 \tag{22}$$

Equation 21 combined with Eq. 19 yields

$$iKA_1 + A_2' = 0 \tag{23}$$

$$A_1 = \frac{i}{K} A_2' \tag{24}$$

Substitution of Eq. 24 into Eq. 22 yields

$$iA_2 (KU + \beta B_o) - \frac{i}{K} A_2'U' - \frac{i}{K} UA_2''$$

$$+ \frac{i}{K} (A_2'U' + A_2U'') - B_o \frac{\beta}{K^2} iA_2'' = 0 \tag{25}$$

Equation 25 may be written more compactly

$$(U + \frac{\beta B_o}{K})(A_2'' - K^2 A_2) - A_2U'' = 0 \tag{26}$$

Equation 26 was derived for a force-free field. If, instead, there are pressure gradients, then Eq. 14 is replaced by:

$$\vec{j} \times \vec{B} = -\nabla P \tag{27}$$

where P is the scalar pressure. Equation 15 becomes

$$\frac{1}{\mu_o} (\vec{B} \cdot \nabla) \vec{B} - \frac{1}{2\mu_o} \nabla B^2 + \nabla P = 0 \tag{28}$$

Since each of the last two terms is the gradient of a scalar, it follows that

$$(\vec{B} \cdot \nabla) \vec{B} = \nabla \Psi \tag{29}$$

where Ψ is a scalar. In this case, there is no need for W since the configuration need not be force-free. Use of Eq. 29 yields the same relation for A_2 as is obtained in the force-free case (Eq. 26).

Except at the boundaries $y = \pm a$, $U'' = 0$; so Eq. 26 can be solved for A_2.

$$A_2 = S_1 e^{Ky} + S_2 e^{-Ky} \qquad |y| < a \tag{30}$$

$$A_2 = S_3 e^{-Ky} \qquad y > a \tag{31}$$

$$A_2 = S_4 e^{Ky} \qquad y < -a \tag{32}$$

where S_1, S_2, S_3, and S_4 are arbitrary constants.

In order to evaluate these constants, four boundary conditions are needed. Two conditions are obtained directly by noting that A_2 is the amplitude of the perpendicular component of $\vec{B}$ and must therefore be continuous across the boundaries at $y = \pm a$. Applying this condition to Eqs. 30-32 yields the equations

$$S_1 e^{Ka} + S_2 e^{-Ka} = S_3 e^{-Ka} \tag{33}$$

and

$$S_1 e^{-Ka} + S_2 e^{Ka} = S_4 e^{-Ka} \tag{34}$$

The remaining boundary conditions are obtained by integrating Eq. 26 across each boundary. For example, at y = a

$$\left[\left(U + \frac{\beta B_o}{K}\right) A_2' - U' A_2\right]_{a-\varepsilon}^{a+\varepsilon} - \int_{a-\varepsilon}^{a+\varepsilon} \left(U + \frac{\beta B_o}{K}\right) K^2 A_2 dy = 0 \tag{35}$$

Since U and A_2 are finite at the boundary, the integral in Eq. 35 is zero. Hence the quantity D defined by

$$D \equiv \left(U + \frac{\beta B_o}{K}\right) A_2' - U' A_2 \tag{36}$$

is continuous across the boundaries at y = $\pm$ a.

Applying this condition to Eqs. 30-32 and using the definition of U (Eqs. 11-13) yields the following

$$\left(\mu_o j_o a + \frac{\beta B_o}{K}\right) \left[K S_1 e^{Ka} - K S_2 e^{-Ka}\right] - \mu_o j_o \left[S_1 e^{Ka} + S_2 e^{-Ka}\right] = -\left(\mu_o j_o a + \frac{\beta B_o}{K}\right) K S_3 e^{-Ka} \tag{37}$$

and

$$\left(-\mu_o j_o a + \frac{\beta B_o}{K}\right) \left[K S_1 e^{-Ka} - K S_2 e^{Ka}\right] - \mu_o j_o \left[S_1 e^{-Ka} + S_2 e^{Ka}\right] = \left(-\mu_o j_o a + \frac{\beta B_o}{K}\right) K S_4 e^{-Ka} \tag{38}$$

Equations 33, 34, 37 and 38 can now be solved to eliminate the constants S_1 through S_4 and yield a dispersion relation for β as a function of K. The first step is to combine Eqs. 33 and 37 to eliminate S_3

$$S_1 e^{Ka}\left[2Ka + 2\frac{\beta B_o}{\mu_o j_o} - 1\right] = S_2 e^{-Ka} \tag{39}$$

Next Eqs. 34 and 38 are combined to eliminate S_4

$$S_2 e^{Ka}\left[2Ka - 2\frac{\beta B_o}{\mu_o j_o} - 1\right] = S_1 e^{-Ka} \tag{40}$$

Combining Eqs. 39 and 40 yields

$$S_2 e^{3Ka}\left[(2Ka - 1) + 2\frac{\beta B_o}{\mu_o j_o}\right]\left[(2Ka - 1) - 2\frac{\beta B_o}{\mu_o j_o}\right] = S_2 e^{-Ka} \tag{41}$$

$$(2Ka - 1)^2 - 4\frac{\beta^2 B_o^2}{\mu_o^2 j_o^2} - e^{-4Ka} = 0 \tag{42}$$

This may be rewritten as

$$\beta = \pm\frac{\mu_o j_o}{2B_o}\left[(1 - 2Ka)^2 - e^{-4Ka}\right]^{1/2} \tag{43}$$

For a disturbance which is periodic in x, K is real. For $0 < Ka < 0.64$, the expression in the brackets is negative. Hence β is imaginary and, if the negative sign is chosen, the disturbance grows exponentially along z with growth constant β. The expression for β (Eq. 43) is formally related to the Kelvin-Helmholtz dispersion relation (Eq. 1) through the substitutions

$$\omega_s \rightarrow \mu_o j_o \tag{44}$$

$$\omega \rightarrow \beta B_o \tag{45}$$

Thus field-aligned current plays a role analogous to vorticity, while

growth with time (ωt) is replaced by growth with distance along B. These results were arrived at more intuitively by Hallinan et al. (1972).

3.3.2 Current Sheet: Geometrical Interpretation

The derivation in the previous section is modeled on Lord Rayleigh's development of the dispersion relation for the Kelvin-Helmholtz instability (Betchov and Criminale, 1967). This approach was chosen because of the observational fact that auroral spirals have the same appearance (geometry) as do fluid vortices. Hence it was evident that the equations governing the vector fields in the two situations must be formally related.

The approach used demonstrates the parallel roles played by vorticity in a fluid and by current in a magnetic field. The magnetic field becomes wrapped around local centers of current just as fluid streamlines wrap around local centers of vorticity.

However, while the perturbation quantities are magnetic field components, the real interest is in the geometrical distortions of the current sheet which produce these field perturbations. In order to gain a better understanding of the field perturbations, consider a current sheet distorted as in Fig. 12.

Each surface of the sheet is described by a sine wave. The two sine waves are assumed to have the same wave number K, but different amplitudes and phases. The equation for the surface at y = a is

$$y_1 = a + C_1 e^{i(Kx + \beta z)} \tag{46}$$

The surface at y = - a is described by

$$y_2 = -a + C_2 e^{i(Kx + \beta z)} \tag{47}$$

Due to the rippling of the current sheet, there is an effective perturbation surface current distribution in the z direction as shown in Fig. 12. The z component of the surface current at y = a is

$$j_z\Big|_{y = a} = -j_o C_1 e^{i(Kx + \beta z)} \tag{48}$$

At y = - a, the z component of the surface current is

$$j_z\Big|_{y = -a} = j_o C_2 e^{i(Kx + \beta z)} \tag{49}$$

If Fig. 12 is to be a valid picture of what a cross section of a current sheet might actually look like, it is necessary that Eqs. 48 and 49 which are derived from this figure be consistent with the perturbation fields derived in Section 3.3.1. Since only the z component of the surface current is specified, only the z component of $\nabla \times \vec{B}$ need be considered. Since the perturbation current is confined to the surfaces, it follows that

$$\left[\nabla \times \vec{B}\right]_z = 0 \qquad \text{or} \quad \begin{matrix} y > y_1 \\ y < y_2 \end{matrix} \tag{50}$$

$$\left[\nabla \times \vec{B}\right]_z = -\mu_o j_o \qquad y_2 < y < y_1 \tag{51}$$

Equation 50 may be rewritten

$$iKA_2 - A_1' = 0 \tag{52}$$

Since $|y| > a$, U' and W' are zero in Eq. 17. Furthermore, W is ignored in comparison to B_o.

$$iA_2 (KU + \beta B_o) - UA_1' - B_o A_3' = 0 \tag{53}$$

From Eq. 21

$$A_3' = \frac{\beta}{K} A_1' \tag{54}$$

Combining Eqs. 53 and 54 shows that Eq. 52 and hence Eq. 50 is valid outside the beam.

Inside the beam Eq. 51 can be written as

$$\left[iKA_2 - A_1'\right] = 0 \tag{55}$$

Equations 17 and 20 can be combined to yield

$$iKA_2(U + \frac{\beta}{K} B_o) - UA_1' - U'A_1 - B_o A_3' = 0 \tag{56}$$

From Eq. 21 (neglecting W)

$$B_o A_3' = -\frac{i}{K} A_2'U' - \frac{i}{K} A_2 U'' + B_o \frac{\beta}{K} A_1' \tag{57}$$

Combining Eqs. 56 and 57 and noting that U'' = 0

$$iKA_2 (U + \frac{\beta}{K} B_o) - UA_1' - U'A_1 + \frac{i}{K} A'_2 U' - B_o \frac{\beta}{K} A_1' = 0 \tag{58}$$

$$\left[iKA_2 - A_1'\right] \quad (U + \frac{\beta}{K} B_o) = U' \quad \left[A_1 - \frac{i}{K} A_2'\right] \tag{59}$$

By the use of Eq. 24 this can be changed to

$$\left[iKA_2 - A_1'\right] \quad (U + \frac{\beta}{K} B_o) = 0 \tag{60}$$

Thus Eq. 51 is validated. The z component of $\nabla \times \vec{B}$ has the required values inside and outside the beam. It remains only to consider the boundaries at $y = \pm a$. A_1, which is the x component of $\vec{B}$, must have a discontinuity at each boundary equal to μ_o times the surface current. This provides two equations which can be used to solve for C_1 and C_2. First it is noted from Eq. 24 that

$$A_1 = \frac{i}{K} A_2' \tag{61}$$

Equations 30-32 are used for A_2' and the surface currents are given by Eqs. 48 and 49. At $y = a$

$$\frac{i}{K}\left[KS_1 e^{Ka} - KS_2 e^{-Ka}\right] - \frac{i}{K}(-KS_3 e^{-Ka}) = -\mu_o j_o C_1 \tag{62}$$

Equation 62 combined with Eq. 33 yields

$$2iS_1 e^{Ka} = -\mu_o j_o C_1 \tag{63}$$

at $y = -a$

$$-\frac{i}{K}\left[KS_1 e^{-Ka} - KS_2 e^{Ka}\right] + \frac{i}{K} KS_4 e^{-Ka} = \mu_o j_o C_2 \tag{64}$$

Equation 64 combined with Eq. 34 yields

$$2iS_2 e^{Ka} = \mu_o j_o C_2 \tag{65}$$

Finally, the amplitude ratio C_1/C_2 is obtained from Eqs. 63 and 65

$$\frac{C_1}{C_2} = -\frac{S_1}{S_2} \tag{66}$$

This can be expressed in terms of β and K by means of Eq. 40

$$\frac{C_1}{C_2} = e^{2Ka}\left[2Ka - 1 - 2\frac{\beta B_o}{\mu_o j_o}\right] \tag{67}$$

where $\frac{\beta B_o}{\mu_o j_o}$ is given as a function of Ka by Eq. 43.

The significant feature of Eq. 67 is that when β is imaginary (modes which grow or decay with distance), C_1/C_2 is a complex number with unity magnitude. Hence the two surface waves have equal amplitudes, but they are not in phase. If the surface wave at y = a lags that at y = - a by x_o (Fig. 13) then C_1/C_2 is related to x_o by the equation

$$\frac{C_1}{C_2} = e^{-iKx_o} \tag{68}$$

In Fig. 14, the quantities $\frac{i\beta B_o}{\mu_o j_o}$ and Kx_o/π are each plotted as a function of $Ka = 2\pi a/\lambda$.

The significant features of Fig. 14 are:

1) Growth occurs for wavelengths such that Ka is between 0 and 0.64. The wavelength to thickness ratio ($\lambda/2a$) varies from

4.9 to infinity.

2) The phase angles corresponding to growing modes are all between 0 and π. Reversing either B_o or j_o would reverse the sign of Kx_o and hence result in phase angles between π and 2π.

3) Large ratios of $\lambda/2a$ correspond to small values of Kx_o. Hence, for a given sheet thickness, the longer wavelength disturbances should form more nearly antisymmetric distortions than do shorter wavelengths. Maximum growth occurs near $Ka = 0.4$ ($\lambda/2a = 7.9$). Here the value of Kx_o is 0.35π (63^o). Rather than folds, the current sheet is distorted into a series of asymmetric bulges.

4) For very short wavelengths ($Ka > 0.64$) β is real and there is neither growth nor damping. Oscillations (as a function of z) can occur, but since there is no growth they should not reach observable magnitudes. For these wavelengths, C_1/C_2 is negative and real, but not equal to 1, i.e., the phase Kx_o is π but the amplitude is greater on one side of the sheet than the other. As an example, letting $Ka = 1$ results in $-C_1/C_2 = 14.7$ or $-C_1/C_2 = 0.068$ depending on the sign of β. The larger value of $-C_1/C_2$ corresponds to the situation where disturbance is primarily on the surface at $y = a$. The lines of constant phase ($Kx + \beta z$ = constant) are parallel to the magnetic field lines located at $y \approx a/2$. As the wavelength becomes still smaller, the disturbance is increasingly confined to a single surface and the lines of constant phase more closely approximate the field lines at that surface.

3.3.3 Long-Wavelength Limit

From the foregoing discussion, it is clear that Fig. 12 represents the long wavelength limit (Ka → 0). In this limit, the disturbance is nearly anti-symmetric. Further insight into the physical mechanism for vortex development can be provided by examining various phase relationships in this limit. First, the limiting value of β is obtained from Eq. 43.

$$\lim_{Ka\to 0} \beta = \lim_{Ka\to 0} -\frac{\mu_o j_o}{2B_o}\left[1 - 4Ka + 4K^2a^2 - 1 + 4Ka - \frac{16K^2a^2}{2}\right]^{\frac{1}{2}} \tag{69}$$

$$\lim_{Ka\to 0} \beta = -\frac{i\mu_o j_o Ka}{B_o} \tag{70}$$

From Eq. 67

$$\lim_{Ka\to 0} \frac{C_1}{C_2} = \lim_{Ka\to 0} -(1 + 2Ka)(2Ka - 1 + 2iKa) \tag{71}$$

Therefore

$$\lim_{Ka\to 0} \frac{C_1}{C_2} = \lim_{Ka\to 0} (1 - 2iKa) = 1 \tag{72}$$

The ratio A_1/C_1 at $y = a + \varepsilon$ is obtained from Eqs. 24 and 31

$$\left.\frac{A_1}{C_1}\right|_{y = a+\varepsilon} = -i\frac{S_3}{C_1}e^{-Ka} \tag{73}$$

Combining this with Eq. 33 yields

$$\left.\frac{A_1}{C_1}\right|_{y = a+\varepsilon} = -i\left[\frac{S_1}{C_1}e^{Ka} + \frac{S_2}{C_1}e^{-Ka}\right] \tag{74}$$

This can be combined with Eqs. 63, 66 and 72

$$\left.\frac{A_1}{C_1}\right|_{y = a+\varepsilon} = i\frac{\mu_o j_o}{2i} + i\,\frac{S_2}{S_1}\,\frac{\mu_o j_o}{2i}\,e^{-2Ka} \tag{75}$$

$$\lim_{Ka\to 0}\left.\frac{A_1}{C_1}\right|_{y = a+\varepsilon} = \lim_{Ka\to 0}\frac{\mu_o j_o}{2}\left[1 - (1 + 2iKa)(1 - 2Ka)\right] \tag{76}$$

$$\lim_{Ka\to 0}\left.\frac{A_1}{C_1}\right|_{y = a+\varepsilon} = \mu_o j_o\, Ka\,(1-i) \tag{77}$$

$$\lim_{Ka\to 0}\left.\frac{A_1}{C_1}\right|_{y = a+\varepsilon} = \mu_o j_o\, Ka\,\sqrt{2}\,e^{-i\pi/4} \tag{78}$$

The x component of the field can be obtained from Eq. 61

$$\frac{A_2}{A_1} = -\frac{iKA_2}{A_2'} \tag{79}$$

A_2 is obtained from Eq. 31

$$\left.\frac{A_2}{A_1}\right|_{y = a+\varepsilon} = i \tag{80}$$

Hence

$$\lim_{Ka\to 0}\left.\frac{A_2}{C_1}\right|_{y = a+\varepsilon} = \mu_o j_o\, Ka\,(i + 1) \tag{81}$$

$$\lim_{Ka\to 0}\left.\frac{A_2}{C_1}\right|_{y = a+\varepsilon} = \mu_o j_o\, Ka\,\sqrt{2}\,e^{i\pi/4} \tag{82}$$

Similarly it can be shown that

$$\lim_{Ka\to 0} \frac{A_1}{C_1}\Big|_{y = -a-\varepsilon} = \mu_o j_o \, Ka \, \sqrt{2} \, e^{i\pi/4} \tag{83}$$

and

$$\lim_{Ka\to 0} \frac{A_2}{C_1}\Big|_{y = -a-\varepsilon} = \mu_o j_o \, Ka \, \sqrt{2} \, e^{-i\pi/4} \tag{84}$$

It can be seen from equations 78, 82, 83 and 84 that A_2 and A_1 each have the amplitude $\mu_o j_o \, Ka \, \sqrt{2} \, C_1$ just outside either surface of the current sheet. The various phase relationships are complicated, but the composite field is illustrated by the arrows in Fig. 12.

A striking feature of Fig. 12 is that in the region near $Kx = \frac{3\pi}{4}$ on the upper surface and near $Kx = \pi/4$ on the lower surface the x and y components of the perturbation field appear to converge. Since the divergence of $\vec{B}$ is everywhere zero, it follows that in these regions the z component of $\vec{B}$ increases as a function of z. To check this, the ratio A_3/C_1 will be evaluated at $y = a+\varepsilon$. First it is noted that $U' = 0$ at $y = a+\varepsilon$ and hence from Eq. 21

$$A_3 = \frac{\beta}{K} A_1 \tag{85}$$

$$\lim_{Ka\to 0} \frac{A_1}{C_1} = \lim_{Ka\to 0} \frac{\beta}{K} \frac{A_1}{C_1} \tag{86}$$

Equation 70 is used for the limiting value of β while Eq. 77 provides the limiting value of A_1/C_1

$$\lim_{Ka\to 0} \frac{A_3}{C_1}\Big|_{y = a+\varepsilon} = -\frac{i\mu_o^2 j_o^2 K^2 a^2}{KB_o} \, (1 - i) \tag{87}$$

$$\lim_{Ka \to 0} \frac{A_3}{C_1}\Big|_{y = a+\varepsilon} = \frac{\mu_o^2 j_o^2 K^2 a^2}{KB_o} \sqrt{2}\ e^{i5\pi/4} \tag{88}$$

Hence B_z has its maximum value at $Kx = 3\pi/4$ as predicted from the convergence of the x + y components of the perturbation field.

It now becomes clear how the disturbance grows with distance along z. There are points of accumulation at $y = a$, $Kx = 3\pi/4$ and at $y = -Kx = \pi/4$. The field lines (and current lines) collect along the surfaces at these two points, resulting in a general thickening of the current sheet in the region between $Kx = 0$ and $Kx = \pi$. This thickening becomes more pronounced as z increases.

The ripple results in a thickening and consequent increase in current near $Kx = \pi/2$, $5\pi/2$, etc. The circular magnetic field resulting from each of these current enhancements is clockwise. The result of these clockwise fields combined with $\vec{B}_o$ is that the amplitude of the initial ripple grows as a function of z.

A periodic ripple in the sheet produces period thickenings which in turn enhance the initial ripple. Consequently, the disturbance grows exponentially with distance.

3.3.4 Rotational Sense: The phase relationships discussed in the preceding section imply that the disturbance has an inherent rotational character. The points of accummulation of field lines are always located in the region where the slope of the sine wave ripple is negative. Expressed differently, the local distortions of the current sheet are clockwise with respect to the thickened regions or points of accummulation. Reversing the direction of either $\vec{B}_o$ or $\vec{j}_o$ would reverse this convection.

As seen in Fig. 13, the phase shift Kx_o between y_1 and y_2 also results in thickened regions in the sheet. Provided that Kx_o is between 0 and π, the thickened regions are on the negative slopes as are also the points of accummulation. The larger the phase angle, the greater the thickening and consequently the larger the value of $|\beta|$.

This relationship holds (see Fig. 14) until Ka reaches 0.4. At this point Kx_o is 63.57^o and the angle between A_3 and y_1 is 116.43^o. The point of accummulation at y = a is directly above the maximum negative excursion in the surface y_2. At larger values of Kx_o (corresponding to larger values of Ka) the growth constant β decreases.

3.3.5 Qualitative Description: In order to see qualitatively how the spirals come about, consider Fig. 15. The upper end of the current sheet is shown in cross section in Fig. 15A. It is uniform along the x axis except for an inifinitesimal perturbation in the form of a current enhancement at x = 0. The dashed lines show the x and y components of the magnetic field. The key elements are a circular field around the current enhancement and the shear field which reverses direction from one side of the current sheet to the other.

By following the field lines which constitute the current sheet, one finds that at some distance $z = z_1$, the sheet is distorted as in Fig. 15B (exaggerated). This distortion is a consequence of the fact that the field lines near x = 0 have components in the y direction. Since the current is antiparallel to $\vec{B}$, the current sheet is distorted in the same manner as the field lines. (If $\vec{B}$ were reversed, as in the Southern Hemisphere, in going from z = 0 to $z = z_1$, one would trace the field lines antiparallel to $\vec{B}$. Consequently, although the field perturbations are in the same direction as in the Northern Hemisphere, the

current sheet would be distorted in the opposite direction. In either case, an upward current implies clockwise distortions as viewed anti-parallel to $\vec{B}_0$.)

In the region where x is slightly less than zero ($z = z_1$, Fig. 15B) the sheet is distorted into that portion of the shear field which is directed in the plus x direction. Similarly, at x somewhat greater than zero, the relevant field lines have x components directed in the -x direction. Consequently, the horizontal components of the field lines are converging toward x = 0. At $z = z_2$ (Fig. 15C) there is a further distortion of the ripple, and there is a further enhancement of the magnetic field and of the current at x = 0.

The initial perturbation is in the form of a current enhancement at x = 0, z = 0. The result is a further enhancement at x = 0, $z = z_2$. Therefore the perturbation continues to grow as a function of z. At $z = z_3$, the fold has evolved into a vortex. The magnetic field lines that have been drawn into the spiral have left deficiencies at values of x somewhat greater than the spiral radius. These deficiencies constitute perturbations which result in additional vortices. In this manner a single initial perturbation can initiate a vortex street as shown in Fig. 15D. The spirals, as seen antiparallel to $\vec{B}$, are clockwise. Reversing either $\vec{B}$ or $\vec{j}$ would reverse the rotational sense.

Figure 15, of course, shows everything in schematic form. Except in the long wavelength limit, the initial stages actually should appear more as bulges than folds.

3.3.6 Alternate Derivation

In treating a related problem, Murty (1961b) used a quite different approach. He considered a slab of an incompressible, inviscid

fluid of low electrical conductivity σ and finite density ρ. The sheet carries a uniform current j_o produced by external sources and is initially parallel to a magnetic field B_o. Murty assumed that $\nabla \times \vec{j} = 0$, basing his assumption on the low conductivity. However, after neglecting small terms, this assumption is also consistent with the magnetic field configuration in Section 3.3.1.

Murty's solution was for a time-dependent problem and is dominated by inertial effects. Furthermore, he made no references to the concept of magnetic shear. Nor did he explicitly recognize that vortices are the logical end result of the instability.

Nonetheless, as is shown in Appendix III both the Kelvin-Helmholtz relation (Eq. 43) and the amplitude ratio (Eq. 67) can be derived from Murty's results by letting $\omega = 0$ and seeking equilibrium solutions.

3.3.7 Nonlinear Development

The derivations for β show clearly that in the linear regime the magnetic shear associated with a current sheet behaves the same as does fluid shear. These equations, of course, break down in the nonlinear limit since sinusoidal perturbations are assumed and second order quantities are neglected. However, the same fundamental equations (Eqs. 18 and 29) which govern $\vec{B}$ also govern the velocity $\vec{V}$ in an incompressible inviscid fluid in equilibrium.

The equation for conservation of momentum in a fluid is:

$$\frac{d\vec{V}}{dt} = \frac{\partial \vec{V}}{\partial t} + (\vec{V} \cdot \nabla)\vec{V} = -\frac{1}{\rho}\nabla P \qquad (89)$$

In the stable limit ($\frac{\partial \vec{V}}{\partial t} = 0$), Eq. 89 is equivalent to Eq. 29. The

equation of incompressibility is

$$\nabla \cdot \vec{V} = 0 \tag{90}$$

which is directly analogous to Maxwell's law (Eq. 18).

Since $\vec{B}$ and $\vec{V}$ satisfy the same basic equations, which are correct to all orders, one can extend the results beyond the linear dispersion relation. The equilibrium current sheet, having sufficient current density (j_o) and sufficient length (ℓ) along z, must be distorted into a vortex street at its free end. The vortex street must be identical in shape to those that occur in inviscid incompressible fluid shear layers.

CHAPTER 4

A MODEL FOR AURORAL ARCS

4.1 Introduction

The next step in discussing the role of shear in auroras is to propose a model based on the developments in Chapter 3. After justifying the underlying assumptions for the model, it will be compared to the morphology described in Chapter 2. Finally, the observations and theory will be combined to make specific estimates of the Birkeland current density and direction and of the magnitude and direction of the perpendicular electric field in particular auroral situations.

4.2 The Model

The ideas discussed in the previous sections can be easily assembled into a model of auroral arcs. The model can then be compared to observations. First, it is assumed that the model arc is an upward directed current sheet aligned along the auroral oval and parallel to the earth's magnetic field. Furthermore, for unknown reasons, this current sheet tends to subdivide into thinner and more intense sheets. These sheets within the overall arc are seen visually as arc elements (Maggs and Davis, 1968).

The intensity of the current within the thin sheets corresponding to the arc elements is sufficient to result in the formation of local V-shaped oblique shocks or double layers as described by Swift et al. (1975). The equipotentials are slightly inclined with respect to the magnetic field and are in the shape of a V centered on the current sheet. Within and above the shock, the current sheet is transformed into a negative charge sheet. For convenient reference, this equipotential

configuration is referred to as a V-layer or V-shock. The larger arc, which contains the arc elements, produces a wider, shallower V-layer.

Within this framework, one can identify several more-or-less distinct stages of activation of the arc.

4.2.1 Quiet Homogeneous Arc

The arc is presumably carrying an upward current, but not of sufficient intensity to cause noticeable distortions in the magnetic field-controlled geometry. V-shocks probably do not form. If they do form, they are weak and the associated perpendicular electric fields are not consequential. Close examination of the arc with sensitive TV cameras reveals that it is already dividing into arc elements and that there are some motions, but the general appearance is relatively quiet.

4.2.2 Rayed Arc

Here the upward current is beginning to cause distortions in the current sheet, creating a slightly wavy appearance in the arc. There are still no large-scale folds or spirals. The current density in some of the arc elements has crossed the threshold for V-shock formation. The V-shocks have strong local counterclockwise vorticity because of the inward directed component of the electric field. This vorticity is evidenced by the formation of curls and also by the rapid motions of the curls. Seen from the side, the curls appear as field-aligned rays.

4.2.3 Spiral

The current is now sufficiently intense to produce major deformations in the arc. One or more clockwise spirals are visible. At some points the arc is displaced hundreds of kilometers from its quiescent position. The inclination of the magnetic field may be altered by as much as 0.5^{o}. The small counterclockwise curls within the large clockwise

spiral indicate very strong V-shocks with intense perpendicular electric fields. At times, individual arc elements try to form smaller spirals, but these short wavelengths are suppressed by the counterclockwise shear from the V-shocks. Instead, somewhat longer-wavelength clockwise folds are formed. When the balance between clockwise shear (current) and counterclockwise shear (charge) changes, the clockwise folds often change abruptly to counterclockwise curls.

4.3 Assumptions

The existence of current sheets corresponding to the arcs and their tendency to subdivide into thinner sheets (arc elements) are basic assumptions. These assumptions are justified by comparing their consequences (formation of spirals, folds, and curls) with observed auroral morphology. In addition, relevant *in situ* measurements are discussed later.

Of more immediate concern are the simplifying assumptions used in the derivation of the current sheet form of the Kelvin-Helmholtz dispersion relation (Eq. 43). These are: 1) The externally imposed magnetic field is straight and uniform; 2) The shape of the current sheet has no temporal dependence; 3) There is a location ($z = 0$) at a distance ℓ from the earth where the current is confined to a flat sheet without distortions.

4.3.1 External Magnetic Field

The relevant distances along the field lines are much too large to justify the approximation of a straight and uniform magnetic field. The field lines have curvature, and both the magnitude of B and the thickness of the current sheet vary along z.

The curvature of the field lines does not introduce any new physics into the problem. Mathematically, each field line can be approximated by a number of straight line segments. A new coordinate system with $\vec{z}$ parallel to $\vec{B}_o$, is associated with each segment. Equation 43 is valid within each segment, and the disturbance amplitude at the end of each segment is used as an initial condition for the following segment. The disturbance still grows as $e^{i\beta z}$ provided that z is now interpreted as a line integral of the distance along $\vec{B}_o$.

The fact that $|B|$ changes drastically along z would be disturbing except for the fact that B appears in the equations (e.g., Eq. 43) in the ratio j_o/B_o. Since the current follows the field lines, this ratio is constant along z.

The most significant variation is that of the product $Ka = 2\pi a/\lambda$. The ratio $\lambda/2a$ cannot be constant because there are different scale factors for mapping latitudinal and longitudinal distances to the equatorial plane (Davis, 1971). For maximum growth, this ratio should be near 8 (Fig. 13). If $\lambda/2a$ is eight at the equatorial plane, it is roughly 32 at the ionosphere (Fairfield, 1968).

The variation of Ka as a function of z does not affect the qualitative conclusions, but it does indicate that the ratio $\lambda/2a$, as observed at the 100-km level, should be $\sim$16-32 rather than $\sim$8. This value agrees with the measured range of 17 to 23. (Hallinan and Davis (1970) reported that a typical value of $\lambda/2a$ for curls is $\sim$16. This may imply that curls, like spirals, originate at large distances from the earth.) Furthermore, the value of β decreases from its maximum at large distances from the earth to somewhat smaller values near the ionosphere. The main consequence is that the required value of j_o may be somewhat greater

than the value calculated from Eq. 43.

4.3.2 Temporal Changes

Equation 43 is a steady-state solution giving the equilibrium configuration of a current sheet. However, many observed spirals are not quiescent. As long as the current density changes sufficiently slowly, the current sheet can be regarded as being continuously in equilibrium. Equation 43 then defines the instantaneous configuration appropriate to the instantaneous current. If the current is increasing, $|\beta|$ is increasing, and hence the spiral is winding up. Conversely, if the current is decreasing, the spiral is unwinding. The definition of "sufficiently slowly" is that the $\vec{j} \times \vec{B}$ force required to accelerate the plasma as the field lines wind up or unwind is small compared to terms of order $A_1 U$. If the current density is changed instantaneously, there may be a period in which Eq. 43 does not apply, but the current sheet will evolve toward the new equilibrium configuration. The rate of change (ω) is given by Murty (1961b) for the mercury sheet, but it has not been calculated for the magnetosphere.

4.3.3 Flat Boundary at z = 0

The assumption of a flat boundary at z = 0 is closely related to that of time independence. If all observed changes are due to changes in β rather than to direct temporal dependence, it follows that at z = 0 the shape of the current sheet is time-independent. There is no reason to assume that this time-independent sheet has any significant distortions.

4.4 Spirals

If the auroral spirals result from Birkeland currents, it follows that these currents are coincident with the discrete aurora, are directed upward, are concentrated near the poleward boundary of the oval, and

occur most often in the evening and midnight sectors.

The current density may be estimated by setting as a threshold condition that an e-fold increase of the perturbation occurs along the length of the field line. This condition can be expressed as:

$$|\beta \ell| \geq 1 \tag{91}$$

where ℓ is the available field line length between the equatorial plane and the earth or between the current source and the earth. The value of ℓ is quite variable and is not at all certain, but 80,000 km serves as a conservative estimate. Combining Eq. 91 with Eq. 43, and assuming that Ka = 0.4, yields a threshold value for j_o of 2.5×10^{-6} amp/m^2. Based on experiments with the similar charge sheet instability (Kyhl and Webster, 1956), it is concluded that formation of a fully-developed spiral requires approximately three times the threshold current. Hence j_o is estimated to be $>7.5 \times 10^{-6}$ amp/m^2 for spiral formation. If the spiral forms in an arc of order 10 km thickness, the total lineal current density is of order 0.08 amp/m. If the spiral forms in an arc system of width 100 km, the lineal current density is of order 0.8 amp/m.

4.5 Folds

The pertinent observations are:

1) Folds are clockwise.

2) They both wind up and unwind.

3) They have wavelengths intermediate between those of curls and of spirals.

4) They are often observed to be in a sort of "tug of war" with the counterclockwise curls.

The clockwise skew of the folds clearly identifies them as a shear type of distortion. Since they have the same rotational sense as spirals and, like the spirals, are reversible, it is reasonable to attribute them to magnetic shear.

Like curls, the folds normally occur in arc elements (small half thickness "a"). However, the folds tend toward longer wavelengths (small K) than do curls. It can be seen from Fig. 14 that, in the linear regime, low values of Ka correspond to nearly anti-symmetric disturbances (Kx_o is small). The frequent occurrence of nearly anti-symmetric folds having relatively small values of Ka suggests to this author that the symmetry of the linear analysis tends to survive in the nonlinear regime as well.

The apparent opposition between folds and curls may result from the fact that the wavelength domains of the two phenomena are not well separated. The short wavelengths, which are close to the typical wavelengths of curls, are apparently suppressed by the opposing counterclockwise shear. As a result, the dominant wavelengths have a relatively small value of Ka and are nearly anti-symmetric.

4.6 Curls Within Spirals

It is an interesting paradox that counterclockwise curls occur regularly within clockwise spirals. It was seen earlier that this inherent conflict between clockwise and counterclockwise shear may play an important role in the formation of folds.

The paradox is easily resolved since two vortex forming mechanisms can exist in a magnetic field. The upward current sheet bends the field lines to produce clockwise vortices (spirals) while a negative charge sheet produces fluid shear which leads to counterclock-

wise vortices (curls).

As described earlier, the current sheet is not an instability as such, but it is rather an equilibrium configuration ($\omega = 0$) which includes spirals at one end. Apparent temporal changes result from variations in the current density. Hence, although the shapes of the spirals and folds are clockwise, their motions can be either clockwise or counterclockwise--or they can be stable (no rotational motion).

The charge sheet, on the other hand, is inherently unstable (negative imaginary ω). Regardless of the temporal changes in the charge density, the curls grow with time. The value of ω changes with the charge density, but there is always growth. Hence curls in the aurora never unwind. All rotational motions of curls are counterclockwise. This is why Oguti (1975) noted only counterclockwise (clockwise in his reference system) motions. (In my viewing of his data, I noted occasional larger scale clockwise motions as well, but the counterclockwise motions are more consistent and are of much higher speed).

The shapes and rotational motions of curls are readily explained by assuming that each discrete arc element is a sheet of negative charge (potential minimum). Furthermore, the translational motions can be explained as the $\vec{E} \times \vec{B}$ drift within one arc element resulting from the electric field produced by the neighboring element. The electric field values required for the translational motions are compatible with those required for the rotational motions (Hallinan and Davis, 1970). However, the assumption of negative charge sheets has other basis. Such charge sheets arise as a natural consequence of current sheets.

When field-aligned currents exceed a critical value, regions of excess charge can appear with consequent electric fields parallel to the

magnetic field (Block and Fälthammer, 1968; Block, 1972; Carlqvist, 1972). These have been referred to as double layers, although the term is somewhat misleading when applied to situations in which the current is localized. Swift (1975) used the term shock for this phenomenon. Kan (1975) reserves the term shock for potential jumps which are supported by the kinetic energy of the ions and continues to use double layers for potential jumps supported by an applied voltage source.

If the Birkeland current is confined to a sheet, the existence of parallel electric fields in the shock or double layer implies that there are perpendicular electric fields above the double layer (Block, 1969; Carlqvist and Bostrom, 1970). The existence of the perpendicular electric field can be readily demonstrated by applying Kirchoff's law to a closed rectangular loop that has one leg in the current sheet and one leg parallel to, but outside of, the current sheet. An upward current causes an upward electric field which accelerates electrons downward and which implies an inward electric field above the shock. In other words, when an upward current sheet exceeds a critical value it becomes a negative charge sheet as well.

The critical value is reached when the electron streaming velocity exceeds the electron thermal velocity (Swift, 1975; Block, 1975). Block (1975) showed that in a typical magnetospheric ionospheric model, this critical current has its lowest value near 3,000 km where it is approximately 2×10^{-5} amp/m^2 locally. This corresponds to $\sim 6 \times 10^{-5}$ amp/m^2 referenced to the 100 km level. Swift (1975) assumed a current of order 8×10^{-6} amp/m^2 and concluded that shocks could form above 1,000 km--most probably between 2,000 km and 3 Re.

Swift (1975) provided a better mathematical foundation for this

picture of combined parallel and perpendicular electric fields by demonstrating that an oblique current driven shock is a self-consistent solution to the Poisson-Vlasov equations. Swift et al., (1975) used the concept of oblique shocks to construct an equipotential model for auroral arcs in which the arc is both a current sheet (upward) and a charge sheet (negative). They discussed in some detail the various observational evidence which supports this model. Block (1975) discusses some of the same evidence.

The fact that curls are small-scale is a necessary consequence of the double layer concept. The potential drop along any field line through the double layer is limited by the available electromotive force (V_o) which drives the current system. If the field-aligned voltage (V_{DL}) within the double layer approaches V_o, the current ceases. Hence the greatest possible magnitude for the potential minimum at the center of the charge sheet is V_o. For a sheet of thickness 2a the maximum value of shear is given by

$$\omega_{s(max)} = \frac{2V_o}{a^2} \tag{92}$$

It follows from Eq. 92 that the electrostatic shear is large compared to the magnetic shear only if a is small, i.e., curls can occur only in arc elements, not in arcs or arc systems.

Another way of looking at this is to note that the V layer concept inherently requires regions of excess positive charge outside the V. While the magnitude of vorticity within a V layer corresponding to an individual arc-element may be quite large, the average charge density over a region substantially larger than the arc-element is small.

Hence the average electrostatic vorticity over large scale-sizes is relatively small.

The main point, as far as this thesis is concerned, is that the small-scale counterclockwise curls are entirely consistent with the large-scale clockwise spirals, even to the extent that the curls themselves can be regarded as indirect evidence of upward current sheets.

4.7 Measurements of Birkeland Currents

In the last few years, measurements obtained with satellite-borne magnetometers have demonstrated that field-aligned currents are a persistent feature of the magnetosphere (Zmuda, and Armstrong, 1974; Sugiura, 1975). In one carefully studied example, the current reached a magnitude of $\sim 7 \times 10^{-6}$ amp/m^2 (Armstrong et al., 1975) in narrow sheets and averaged 2×10^{-6} amp/m^2 over a distance of $\sim$200 km. (This implies a lineal density of $\sim$0.4 amp/m.) In the evening sector the current is generally inward on the equatorward side and outward on the poleward side (near the discrete auroras). In the morning this pattern is reversed (Yasuhara, et al., 1975).

However, there are frequent exceptions to this convention. The detailed picture is far more confusing and includes many current sheets in both directions. Due to the limited time resolution of the satellite data, as well as the inability to distinguish fully between spatial and temporal variations, it is not normally possible to correlate specific magnetic field variations observed by the satellite with particular auroral arcs.

In order to confidently measure currents within individual arcs, it is necessary to use sounding rockets rather than satellites. The Rice University group has reported three rocket flights with vector magneto-

meters. In each case, upward Birkeland currents of magnitude sufficient to produce spirals were detected within or at the poleward edge of visible auroral forms (Anderson and Cloutier, 1975). Of particular interest is the flight of February 25, 1972 (Casserly and Cloutier, 1975) which passed through a system of folds or poorly developed spirals in the evening sector. Within the aurora an upward current of 3.3×10^{-5} amp/m^2 was observed. This is roughly five times the calculated value for spiral formation. Kintner et al., (1974) reported a rocket flight which penetrated a large spiral. They interpreted the magnetometer measurements as indicating two upward current sheets of density 5×10^{-6} amp/m^2, one of which coincided with the location of the visible arcs.

A completely different measurement technique was used by Wescott et al., (1975a) in the so-called "OOSIK" experiment. They employed a shaped explosive charge to eject barium atoms at high velocity parallel to a magnetic field line. The atoms were quickly ionized by sunlight and were consequently confined to the field line. Since the ions were visible from the ground through resonant scattering of sunlight, the effect was to illuminate a large portion of a particular flux tube.

Approximately twenty minutes after injection, a westward travelling surge in the form of a medium-sized spiral passed over Alaska. There was relative motion between the barium and the aurora so that at one point the barium crossed an outer limb of the spiral. A careful observation of the tagged field line showed that it changed orientation as it crossed the aurora. This change in orientation was interpreted as resulting from an upward sheet current within the visible aurora of $\sim 8 \times 10^{-2}$ amp/m.

Since the arc was $\sim$10 km in thickness, this total current implies a

current density of $\sim 8 \times 10^{-6}$ amp/m^2, in good agreement with the magnetic shear theory for spirals.

The rocket measurements reported here all refer to the evening or midnight sectors and they all indicate currents of order 10^{-5} amp/m^2 flowing upward within discrete auroral arcs. These currents are sufficient to produce folds or spirals, and such distortions are observed. The satellite measurements in these sectors, although they cannot be confidently associated with individual arcs, concur to the extent that, generally, the current is upward in the region where discrete auroras are expected (the poleward edge of the evening oval).

In the morning sector, near the dawn meridian, the situation is less certain. There are no relevant rocket flights in this sector, primarily because the discrete auroras at this time are usually too far poleward to reach with rockets from Poker Flat or Ft. Churchill.

The satellite data indicate that the poleward current system in the morning is usually directed downward. However, Yasuhara's Fig. 2.4 (1975) strongly suggests that for moderately disturbed conditions near 06 hours geomagnetic local time there is often a second pair of current sheets poleward of the oval. The more poleward of the pair is directed upward. It is in this region that the morning spirals are observed.

On the basis of these various observations it may be concluded that there is considerable uncertainty regarding the morning sector. Still, the available evidence does not preclude the assumption that all discrete auroras correspond to upward currents.

4.8 Electric Fields

The most controversial part of the charge sheet theory for curls is the requirement that there be perpendicular electric fields of order

500 mv/m (referenced to 100-km altitude). This required field is five-ten times the value of fields typically measured by conventional techniques. As discussed by Swift et al. (1975) and by Block (1975), the solution can be found in the fact that, according to their equipotential models, the large perpendicular fields occur above the double layer (estimated to be ∿3000 km altitude by Block (1975)). Most measurements are made below 1000 km altitude.

However, high-altitude perpendicular fields can be measured with the shaped charge barium technique described earlier. In joint projects between the University of Alaska and Los Alamos Scientific Laboratory, seven shaped charges have been injected on high-latitude field lines. In three of these cases, high-altitude (>3000 km) electric fields in excess of 200 mv/m (referenced to the 100-km level) were detected (Wescott et al., 1975a; Wescott et al., 1975b; E. M. Wescott, private communication). In each case the large field values were closely associated with the visible aurora. In the OOSIK experiment the direction of the electric field reversed as the barium crossed the aurora. The field was pointed toward the aurora throughout the interval, indicating that the aurora, in addition to being an upward current sheet (see earlier discussion of field line orientations), was also a negative charge sheet.

Another shaped charge barium experiment, code named SKYLAB BETA because it was the second of two releases timed to coincide with passes of the NASA SKYLAB, was especially interesting in that the barium streak actually was observed to cut through a double layer (Wescott et al., 1975b). Barium drifts above the double layer indicated electric fields of >200 mv/m (referred to the 100-km level) but the fields below the double layer were ∿40 mv/m. The altitude of the double layer was

∿5,000-6,000 km. At the time of the measurement, the affected field lines were too far from the observing stations to allow detailed description of the aurora. The release was in the morning sector. At the time of interest, the barium streak was near to or coincident with an omega band (O. Røyrvik, private communication) which delineated the poleward boundary of a diffuse region of pulsating aurora.

4.9 Morning Sector Spirals

Comparing theory to observation in the morning sector is difficult as there is a lack of observations. There are no reports of rocket flights carrying vector magnetometers through the discrete morning auroras. Morning shaped charge barium experiments have been at lower latitudes than those at which the morning spirals are observed.

The satellite data, noted earlier, indicate a general pattern of an upward current region equatorward of a downward current region in the morning sector. However, this pattern cannot be identified with individual arcs. Hence there is no direct observational evidence concerning the magnitudes or directions of current sheets associated with discrete arcs in the morning sector.

There is also a lack of information concerning the discrete visual forms in this sector. DMSP images and all-sky photographs are available, but there is no television data or high-time-rate all-sky data. Hence the forms are well documented, but the dynamics are virtually unknown. Specifically, it is not known whether spirals in this region are reversible. Nor is it known whether or not curls occur within these spirals.

Lacking those two pieces of information, it is not possible to state conclusively whether or not these spirals result from magnetic shear. The alternative explanation is that they result from electro-

static shear. The region in which they occur is one in which there is clockwise shear in the global convection pattern (Gurnett and Frank, 1973). Conceivably, this clockwise shear (net positive charge) may somehow impose itself on the precipitating electrons to produce clockwise spirals.

It can be confidently stated, however, that there are no concentrated downward sheet currents associated with the discrete auroras in this sector.

4.10 Birkeland Currents Outside of the Discrete Auroras

The spirals are formed by upward Birkeland currents on the field lines terminating in the discrete auroras. However, some of the rocket measurements also indicate downward currents immediately equatorward of each discrete arc (e.g., Casserly and Cloutier, 1975).

The presence of uniform Birkeland currents outside the discrete arcs has no effect on the linear analysis of Chapter 3. This is because the field within the aurora due to a current sheet outside the aurora is constant and can be combined with B_o by a slight rotation of the coordinate system. However, non-uniformities in the auroral sheet could induce corresponding perturbations in nearby current sheets. These in turn could interact with the auroral sheet to modify the process of spiral formation. A downward current sheet equatorward of the discrete aurora should produce counterclockwise spirals in the magnetic field. These would not be visible since they involve field lines which are not carrying large fluxes of energetic electrons. However, each of these hypothetical reverse spirals would produce shear and hence observable effects within the visible aurora.

The interactions are probably highly non-linear and the detailed

consequences are not easily predicted. However, considerable insight is afforded by the fluid analogy. Homann (1936) photographed the streamlines in the wake behind a circular cylinder in a stream of oil. The result, reproduced from Batchelor (1970), is shown in Fig. 16. In the region downstream from the obstruction, there are two adjacent shear layers with oppositely-directed vortices. This situation is exactly analogous to the pair of oppositely-directed Birkeland current sheets.

By covering the counterclockwise vortex street in Fig. 16, it is presumably possible to determine what auroral spirals should look like if the Birkeland current within the aurora were balanced by an equal and opposite current immediately equatorward of the discrete arc. The shape of the individual spirals is not substantially modified by the second current sheet. However, adjacent clockwise spirals are no longer connected.

The observed auroral spiral streets usually have a clear connection between adjacent spirals. It would seem, therefore, that the effect of any downward current sheets outside of the discrete auroras is somehow diminished. Possible reasons could be: 1) the downward current has a smaller magnitude or lower density (more spread out) than the upward sheet; 2) there is a substantial space between the two current sheets; 3) the downward current has a substantially shorter pathlength than does the upward current.

The only current measurements known to be directly associated with spirals (Kinter et al., 1974; Wescott et al., 1975a) both indicate a net upward current with no balancing downward current in the immediate vicinity of the discrete aurora.

CHAPTER 5

CONCLUSIONS

The major conclusion of this thesis is that the spirals which form in discrete auroral arcs are (at least in the evening and midnight sectors) the result of the magnetic shear associated with upward directed Birkeland current sheets. Folds are interpreted as also resulting from upward current sheets, but under circumstances such that the modes corresponding to small values of $\lambda/2a$ are suppressed. Curls are attributed to the charge sheet form of the Kelvin-Helmholtz instability. The charge, in turn, is associated with the V-shaped shock or double layer which forms when the Birkeland current exceeds a critical value.

It is compatible with the available evidence to assume that all or most discrete auroral arcs are upward current sheets. The typical current density in the sheets terminating in the discrete auroras is of order 10^{-6} to 10^{-5} amp/m^2 (see Table II).

TABLE II

Type of Measurement or Theoretical Basis	Source	Upward Current Density Referred to 100 km Altitude (amp/m^2)
Threshold for Spiral Formation	This Thesis	2.5×10^{-6}
Fully Developed Spiral	This Thesis	8×10^{-6}
Formation of Charge Sheet (V-shaped double layer)	Block, 1975	6×10^{-5}
Rocket-borne Magnetometer	Cloutier et al. (1970)	2.6×10^{-5}
Rocket-borne Magnetometer	Cloutier et al. (1973)	4×10^{-6}
Rocket-borne Magnetometer	Casserly and Cloutier (1975)	3.3×10^{-5}
Rocket-borne Magnetometer	Kintner et al. (1974)	5×10^{-6}
Shaped Charge Barium	Wescott et al. (1975)	8×10^{-6}
Triad Satellite Magnetometer	Armstrong et al. (1975)	7×10^{-6}

Current densities much below 10^{-6} amp/m^2 should not produce significant distortions in the arcs or cause noticeable rays. Densities much higher than 10^{-4} amp/m^2 would produce unreasonable field line distortion and, furthermore, are probably precluded by the current limiting property of double layers.

The linearized theory contains no information concerning the possibility of downward currents immediately adjacent to the discrete arcs. It is inferred from a fluid analogy that such currents should produce observable effects--they are not normally observed.

Another present limitation to the theory is the uncertainty regarding the cause of the spirals near the dawn meridian. Additional data with better time resolution may solve this problem. The most definite statement that can be made at this time is negative. There is no evidence, in any local time sector, of formations which can be attributed to concentrated downward current sheets coincident with discrete auroras.

The presence of a potential minimum within auroral arcs is indicated by the observations of curls. Their behavior is entirely consistent with the arc being a potential minimum. If the V-layer theory is correct, the presence of curls always indicates an upward current.

The conclusions regarding Birkeland currents and electric fields may be summarized as follows:

1) Most discrete auroral forms are associated with upward currents.

2) No discrete auroral forms are associated with downward currents.

3) Many discrete forms (particularly those in which the current density is high) are associated with negative charge sheets.

4) No discrete auroral forms occurring equatorward of $\sim 67^{\circ}$ latitude are associated with positive charge sheets. (There are few TV observations poleward of this latitude).

5) A typical Birkeland current density for discrete forms is 10^{-5} amp/m^2.

6) A typical perpendicular electric field strength in discrete auroras with curls is 500 mv/m referenced to the 100-km level.

7) The field-aligned potential drop expected in a 10-km thick arc with a 500 mv/m peak perpendicular electric field is $\sim$1.2 kev.

Future Studies

The most pressing need is to remove the uncertainties concerning the high-latitude morning sector. A significant step can be made in this direction by obtaining high exposure rate (>6 frames per minute) all-sky films from a suitable station in order that the dynamics of the spirals can be studied. If the spirals are reversible, they almost certainly result from Birkeland current. If not, $\vec{E} \times \vec{B}$ fluid shear may be responsible. Ideally, this region should also be probed with rocket-borne magnetometers or barium shaped charges.

There also is need for more information concerning double layers in all local-time sectors. At present, the only technique that is known to be suitable for the detection of double layers is the barium shaped charge. It is crucial to monitor the barium streaks over the altitude range 2,000 km to 8,000 km. Although the evidence is less direct, ground-based TV observations of curls provide considerable information concerning possible double layers. At the moment, there is relatively little TV data available from poleward of latitude 67°.

Short-baseline triangulation of auroras using TV cameras is now

being conducted (Brown et al., 1975). This technique makes it possible to measure spatial and temporal variations in auroral altitudes which can, in turn, be related directly to the energy of auroral primaries. Since one of the properties of double layers is that they accelerate electrons, their effects should be measurable with this system.

Ultimately, there is need of continuous imaging of the auroral oval with high temporal and spatial resolution over periods comparable to the duration of magnetospheric substorms. This is possible with present technology by utilizing TV cameras in a satellite with a high-altitude elliptical orbit. This concept has been discussed at length under the acronym "CYCLOPS" (Davis, 1973). The images provided by such a satellite could easily be interpreted to provide a dynamic picture of the development and decay of those portions of the magnetospheric current system that flow on the field lines connected to the discrete visual auroras.

From a theoretical standpoint, the biggest problem is to explain the existence of the auroral arcs. An equally fascinating, although possibly simpler, problem is to explain the tendency to subdivide into arc elements.

The implications of magnetic shear should be considered in other regions of the magnetosphere and in the vicinity of sunspots. Pictures of the solar disc show formations which are remarkably similar to vortex streets.

Since the Kelvin-Helmholtz instability in fluids is usually observed in situations where $\nabla \times \vec{V}$ is perpendicular to $\vec{V}$, it might be useful to extend the mathematics of Chapter 3 to cover situations in which j_o is perpendicular to B_o. There is also need for careful study of

situations in which B_o is small compared to U, e.g., the neutral sheet in the geomagnetic tail. Direct application of Eq. 43 to the neutral sheet would yield an infinite value for β. Of course, this is unrealistic since it was assumed in the derivation of Eq. 43 that $\beta/K \ll 1$ and that $U \ll B_o$. A more realistic expression may well contain interesting insights.

APPENDIX I

List of Symbols

a The thickness of a shear layer, charge sheet, or current sheet is 2a and is measured along the y axis (meters).

A_1, A_2, A_3 Magnetic field perturbation amplitudes in the x,y, and z directions, respectively.

$\vec{B}$ The magnetic field (webers/m^2).

B_o The magnetic field in the absence of current sheets is in the plus z direction (webers/m^2). $B_o = 5 \times 10^{-5}$ weber/m^2 at 100 km altitude.

D Quantity defined by Eq. 33.

$\vec{E}$ Electric field (volts/m).

e Charge on electron (1.6×10^{-19} coulombs).

$\vec{j}$ Field-aligned current density (amp/m^2).

j_o The unperturbed Birkeland current is in the minus z direction.

K Wave number in x (east-west) direction. Real K implies sinusoidal variation.

ℓ Length of field line from equatorial plane to earth.

n_e Electron density (electrons/m^3).

n_i Ion density (ions/m^3).

P Scalar pressure.

S_1, S_2, S_3, S_4 Arbitrary constants.

t Time.

T Surface tension

U Magnetic shear field caused by current sheet--defined by Eqs. 11-13.

$\vec{V}$ Velocity (m/sec).

W Additional magnetic field along z due to currents along x.

$\vec{x}$ Coordinate, positive eastward.

$\vec{y}$ Coordinate, positive southward.

x_o Displacement between two surface waves.

$\vec{z}$ Coordinate, positive out of paper (toward earth).

α Ratio of amplitudes of two surface waves. α is generally a complex number representing a phase shift.

β Growth constant along z; negative imaginary β corresponds to growth.

ε Infinitesimal distance along y.

ε_o Permitivity. 8.85×10^{-12} farad/meter.

θ Phase angle between two surface disturbances--$0 < \theta < 180$ implies clockwise rotation viewed antiparallel to B.

λ Wavelength along x.

μ_o Permeability. 1.257×10^{-6} henry/meter.

ω Growth constant--imaginary ω corresponds to exponential growth (instability).

ω_s The vorticity $\omega_s \equiv \frac{\partial v_x}{\partial y}$.

ρ Mass density.

σ Electrical conductivity.

Ψ Arbitrary scalar function.

APPENDIX II

The Kelvin-Helmholtz dispersion relation (Eq. 1) was derived by Lord Rayleigh on the basis of conservative forces and incompressibility. The two basic fluid equations are:

$$\frac{d\vec{V}}{dt} = -\nabla\Psi \tag{A1}$$

and

$$\nabla \cdot \vec{V} = 0 \tag{A2}$$

The two basic equations governing the charge sheet are different from A1 and A2. They are (Eqs. 7 and 5 from Chapter 3)

$$\nabla \cdot \vec{V}_{\perp} = 0 \tag{A3}$$

and

$$\frac{d}{dt}(\nabla \times \vec{V}_{\perp}) = 0 \tag{A4}$$

where $\vec{V}_{\perp}$ is the guiding center velocity perpendicular to the magnetic field.

In this Appendix, a dispersion relation is derived on the basis of Eqs. A3 and A4. Also, since the laboratory versions of the charge sheet instability (Cutler, 1956; Webster, 1957) show growth as a function of distance rather than of time, this derivation will specifically allow for the possibilities of temporal or spatial growth as well as combinations thereof.

The charge sheet is oriented as in Fig. 11 and the components of velocity are given by:

$$V_x = A_1 e^{i(Kx + \beta z - \omega t)} + U \tag{A5}$$

$$V_y = A_2 e^{i(Kx + \beta z - \omega t)} \tag{A6}$$

$$V_z = A_3 e^{i(Kx + \beta z - \omega t)} + W \tag{A7}$$

$$U = \omega_s y \qquad |y| \leq a \tag{A8}$$

$$U = \omega_s a \qquad y > a \tag{A9}$$

$$U = -\omega_s a \qquad y < -a \tag{A10}$$

The z component of vorticity is

$$\nabla \times \vec{V}_\perp = \left[\frac{\partial V_y}{\partial x} - \frac{\partial V_x}{\partial y}\right] \hat{z} \tag{A11}$$

$$\frac{d}{dt}(\nabla \times \vec{V}_\perp) = \frac{\partial}{\partial t}(\nabla \times \vec{V}_\perp) + (\vec{V} \cdot \nabla)(\nabla \times \vec{V}_\perp) \tag{A12}$$

Equating the right hand side of Eq. (A12) to zero and using the expressions for $\vec{V}$ (Eqs. A5 through A10) yields:

$$-i\omega A_1' - \omega K A_2 + iKUA_1' + K^2 UA_2 + A_2 U'' + i\beta WA_1' + K\beta WA_2 = 0 , \tag{A13}$$

where primes indicate differentiation with respect to y. This expression

may be simplified somewhat by defining

$$\bar{\omega} \equiv \omega - \beta W \ . \tag{A14}$$

Then Eq. A13 can be rewritten

$$(A_1' - iKA_2)(iKU - i\,\bar{\omega}) + A_2 U'' = 0 \ . \tag{A15}$$

Substituting the expressions for $\vec{V}$ into Eq. A3 yields

$$iKA_1 + A_2' = 0 \ . \tag{A16}$$

Substitution of Eq. A15 into Eq. A14 yields

$$(K^2 A_2 - A_2'')(U - \frac{\bar{\omega}}{K}) + A_2 U'' = 0 \ . \tag{A17}$$

Comparison with Eq. 26 in the text shows that Eq. A17 is identical except that βB_o has been replaced by $-\bar{\omega}$. Furthermore, Eq. 43 is derived from Eq. 26 and Eqs. 11-13. Equations 11-13 are identical to Eqs. A8-A10 except that $\mu_o j_o$ is replaced by ω_s. It follows that Eq. 43 may be used with the substitutions:

$$\beta B_o \rightarrow -\bar{\omega} \tag{A18}$$

and

$$\mu_o j_o \rightarrow \omega_s \ . \tag{A19}$$

Hence

$$\bar{\omega} = \omega - \beta W = \pm \frac{\omega_s}{2} \left[(1 - 2Ka)^2 - e^{-4Ka} \right] \tag{A20}$$

In the limit $\beta \to 0$, Eq. A20 reduces to Eq. 1 in the text. The experiments performed by Cutler and by Webster represent the opposite limit $\omega \to 0$. In this case, the growth is convective with growth constant β.

APPENDIX III

The formation of spirals in a current sheet is related to the instability of a current-carrying slab of mercury. Murty (1961b) analyzed the stability of the mercury sheet by considering two geometrical surface perturbations of the form

$$y_1 = a + b \cos \phi \qquad (A_3 1)$$

on one surface and

$$y_2 = -a - \alpha\, b \cos \phi \qquad (A_3 2)$$

on the other surface. The ratio of the amplitudes is α which can be complex. The amplitude of the surface wave at $y = a$ is b and is given by

$$b = b_o \cos \omega t \qquad (A_3 3)$$

The phase factor ϕ is given by

$$\phi = Kx + \beta z \qquad (A_3 4)$$

where K and β are the wave number and the spatial growth constant as in Section 3.3.1. (In the above equations and in the subsequent discussion, Murty's coordinate system has been rotated and quantities relabeled to be consistent with the designations used in the previous section. The transformations are given at the end of this appendix.)

If K is real and β and ω are both imaginary, the disturbance grows exponentially with both time and distance. At t = 0, the sheet is everywhere flat except for an infinitesimal perturbation. At a somewhat later time the sheet is still flat at z = 0, but is distorted at some distance along z. The distortion consists of sine waves (as a function of x) on the two surfaces. At a still later time, the distortion at large z is still greater.

The spatial and temporal growth are more readily visualized by reference to an experiment performed by Dattner (1961). He caused large currents (100 amp - 300 amp) to flow along a vertical column of freely falling mercury. A vertical magnetic field of 300 gauss was externally imposed. In a few milliseconds, the initially straight column distorted into a corkscrew shape, the distortion growing with both time and distance. When a current of 300 amp was used, the corkscrew grew so large that the mercury column broke up.

Murty (1961a) analyzed this situation and then (1961b) extended the analysis to the vertical slab of mercury. He used a magnetostatic approximation in which the curl of j was assumed to be equal to zero. This was justified by the assumption of low conductivity. Consider Maxwell's equation

$$\frac{\partial \vec{B}}{\partial t} = -\nabla \times \vec{E} = -\nabla \times \left[\frac{\vec{j}}{\sigma} - \vec{V} \times \vec{B}\right] \qquad (A_3 5)$$

If $\sigma \to 0$, $\nabla \times \vec{j}$ must also approach zero in order that the first term on the right hand side remain finite.

Murty's solutions for the growth rate ω and the amplitude ratio α are given by Eqs. $A_3 6$-$A_3 14$

$$\omega^2 = \frac{1}{\rho}\left[(1+\alpha)(P+Q) + (1-\alpha)(M+N)\right] \qquad (A_3 6)$$

and

$$\alpha = \frac{1}{\zeta}\left[-\eta \pm (\eta^2 - \zeta\theta)^{\frac{1}{2}}\right] \qquad (A_3 7)$$

where ζ is defined by

$$\zeta \equiv P + Q - M - N \qquad (A_3 8)$$

η is defined as

$$\eta \equiv Q + N \qquad (A_3 9)$$

θ is defined as

$$\theta \equiv Q + M - P - N \qquad (A_3 10)$$

P is defined as

$$P \equiv \left[\tfrac{1}{2} TK^3 + \frac{1}{2}\mu_o j_o^2 (Ka - e^{-Ka}\cosh Ka)\right] \tanh Ka \qquad (A_3 11)$$

Q is defined as

$$Q \equiv \tfrac{1}{2} j_o B_o \beta \coth Ka \qquad (A_3 12)$$

M is defined as

$$M \equiv \left[\tfrac{1}{2} TK^3 + \tfrac{1}{2}\mu_o j_o^2 (Ka - e^{-Ka}\sinh Ka)\right] \coth Ka \qquad (A_3 13)$$

and N is defined as

$$N \equiv \tfrac{1}{2} j_o B_o \beta \tanh Ka \qquad (A_3 14)$$

T is the surface tension, ρ is the density of the fluid, and ω, μ_o, j_o, B_o, K, a, and β have the same meanings as in Section 3.3.1.

Murty's basic assumption ($\nabla \times \vec{j} = 0$) is consistent with the field configuration of Chapter 3 (neglecting the correction term W). Hence there should be consistency between his results and those of Chapter 3. Since Chapter 3 deals with an equilibrium configuration, ω is set equal to zero in Eq. $A_3 6$, yielding

$$(1 + \alpha)(P + Q) + (1 - \alpha)(M + N) = 0 \qquad (A_3 15)$$

Equations $A_3 15$ and $A_3 8$ yield

$$P + Q + M + N + \alpha\zeta = 0 \qquad (A_3 16)$$

Equations $A_3 15$ and $A_3 7$ yield

$$P + Q + M + N - \eta \pm (\eta^2 - \zeta\theta)^{\frac{1}{2}} = 0 \qquad (A_3 17)$$

Equations $A_3 17$, $A_3 8$, $A_3 9$ and $A_3 10$

$$P + M \pm (Q^2 + N^2 + 2QN - 2PM + P^2 - Q^2 + 2QN + M^2 - N^2)^{\frac{1}{2}} = 0 \qquad (A_3 18)$$

This result reduces to:

$$P + M \pm (4QN - 2PM + P^2 + M^2)^{\frac{1}{2}} = 0 \qquad (A_3 19)$$

$$(P + M)^2 = (P - M)^2 + 4QN \qquad (A_3 20)$$

$$PM = QN \qquad (A_3 21)$$

Now substitutute the definitions of P, M, Q and N into Eq. $A_3 21$ and let the surface tension T equal zero

$$\mu_o^2 j_o^2 (Ka - e^{-Ka} \cosh Ka)(Ka - e^{-Ka} \sinh Ka) = B_o^2 \beta^2 \qquad (A_3 22)$$

using the definitions

$$\cosh Ka \equiv \tfrac{1}{2}(e^{Ka} + e^{-Ka}) \qquad (A_3 23)$$

and

$$\sinh Ka \equiv \tfrac{1}{2}(e^{Ka} - e^{-Ka}) \qquad (A_3 24)$$

Equation $A_3 22$ may be simplified

$$\beta = \pm \frac{\mu_o j_o}{2B_o} \left[(1 - 2Ka)^2 - e^{-4Ka}\right]^{\frac{1}{2}} \qquad (A_3 25)$$

Equation $A_3 25$ is identical to Eq. 43, which in turn is formally related to the Kelvin-Helmholtz dispersion relation, as discussed earlier. Murty did not explicitly use the concept of magnetic shear, or for that matter, recognize that the end result of the instability is a vortex

street. However, his equations do predict that while the plane sheet is unstable, it becomes stable ($\omega = 0$) after it has assumed a configuration in which the spatial disturbance grows exponentially along the sheet. The line current analog of this statement is demonstrated by Dattner's Fig. 4 in which the 100 amp current appears to form a stable corkscrew after $\sim$15 msec. Of course, it is not proper to apply Murty's derivation to determine the growth rate (ω) of spirals. However, both Murty's derivation and the shear approach show that the only stable configuration is one which includes vortices at one end of the sheet.

Phase Angle

A distinctive feature of Murty's derivation is that he explicitly considers separate waves on the two surfaces of the sheet. The waves have the same temporal and spatial growth constants (ω, β) and the same wave number (k), but their amplitudes differ by a factor (α) (Eq. $A_3 2$). Murty concluded that in the case of a current slab in a magnetic field, $\alpha \neq \pm 1$. Hence the disturbance is neither symmetric nor antisymmetric with respect to the x-z plane.

By using Murty's equations with $\omega = 0$, it is possible to evaluate α as a function of the wave number (K) and sheet thickness (2a).

Solving Eq. $A_3 15$ for α results in:

$$\alpha = - \frac{P + Q + M + N}{P + Q - M - N} \qquad (A_3 26)$$

Multiplying numerator and denominator by M and using Eq. $A_3 21$ to eliminate P;

$$\alpha = - \frac{QN + QM + M^2 + NM}{QN + QM - M^2 - MN} \qquad (A_3 27)$$

$$\alpha = - \frac{(Q + M)(M + N)}{(Q - M)(M + N)} = - \frac{Q + M}{Q - M} \qquad (A_3 28)$$

The definition (Eqs. $A_3 12$ and $A_3 13$) may be used for Q + M (T = 0)

$$\alpha = - \frac{B_o \beta + \mu_o j_o (Ka - e^{-Ka} \sinh Ka)}{B_o \beta - \mu_o j_o (Ka - e^{-Ka} \sinh Ka)} \qquad (A_3 29)$$

Where ß is given by Eq. $A_3 25$ and the directions of B_o and j_o are as shown in Fig. 12.

By using Eq. $A_3 25$ it may be shown after some algebraic manipulation, that

$$\frac{1}{\alpha} = \left[(2Ka - 1) - \frac{2\beta B_o}{\mu_o j_o} \right] e^{2Ka} \qquad (A_3 30)$$

Comparison with Eq. 67 shows that

$$\alpha = - \frac{C_2}{C_1} \qquad (A_3 31)$$

A comparison between Eq. 46 and 47 on the one hand and Eq. $A_3 1$ and $A_3 2$ on the other shows that the result indicated by $A_3 31$ is consistent. Furthermore, the dispersion relation ($A_3 25$) is identical to Eq. 43.

This correspondence shows that the instability discussed by Murty is actually a Kelvin-Helmholtz type of instability and is closely related to the auroral spirals.

To convert from the symbols used by Murty (1961b) to those used in this thesis, the following substitutions must be made.

Murty (1961b)	→	this paper
z	→	y
y	→	$-z$
x	→	x
d	→	a
a	→	b
a_o	→	b_o
j_o	→	j_o
B_u	→	$-B_o$
K	→	$\frac{}{\sqrt{K^2 + \beta^2}} \quad K$
K_x	→	K
K_y	→	$-\beta$
ϕ	→	$Kx + \beta z$
α	→	$e^{i(Kx_o - \pi)}$
$\alpha \cos \phi$	→	$\cos (\phi + Kx_o - \pi)$

REFERENCES

Akasofu, S.-I. and D. S. Kimball, The dynamics of the aurora - I: Instabilities of the aurora, J. Atmos. Terr. Phys., 26, 205-211, 1964.

Akasofu, S.-I., D. S. Kimball and C.-I. Meng, The dynamics of the aurora - II: Westward traveling surges, J. Atmos. Terr. Phys., 27, 173-187, 1965a.

Akasofu, S.-I., D. S. Kimball and C.-I. Meng, The dynamics of the aurora - III: Westward drifting loops, J. Atmos. Terr. Phys., 27, 189-196, 1965b.

Akasofu, S.-I., R. H. Eather and J. N. Bradbury, The absence of the hydrogen emission (Hβ) in the westward traveling surge, Planet. Space Sci., 17, 1409-1412, 1969.

Akasofu, S.-I., A study of auroral displays photographed from the DMSP-2 satellite and from the Alaska meridian chain of stations, Space Sci. Rev., 16, 617-725, 1974.

Alfvén, H., Cosmical Electrodynamics, Oxford Univ. Press, Oxford, p. 206, 1950.

Anderson, H. R. and P. A. Cloutier, Simultaneous measurements of auroral particles and electric currents by a rocket-borne instrument system: Introductory remarks, J. Geophys. Res., 80, 2146-2151, 1975.

Anger, C. D. and A. T. Y. Lui, A global view of the polar region on 18 December 1971, Planet. Space Sci., 21, 873-878, 1973.

Armstrong, J. C., S.-I. Akasofu and G. Rostoker, A comparison of satellite observations of Birkeland currents with ground observations of visible aurora and ionospheric currents, J. Geophys. Res., 80, 575-586, 1975.

Batchelor, G. K., An introduction to fluid dynamics, Plate 2, Cambridge Univ. Press, Cambridge, 1970.

Betchov, R. and W. Criminale, Jr., Stability of parallel flows, Academic Press, New York and London, 1967.

Block, L. P. and C. G. Fälthammar, Effects of field-aligned currents in the ionosphere, J. Geophys. Res., 73, 4807, 1968.

Block, L. P., Electron and plasma physics, Royal Inst. of Technology, 10044 Stockholm, Sweden, Rept. 69-30, 1969.

Block, L. P., Potential double layers in the ionosphere, Cosmic Electrodynamics, 3, 349-376, 1972.

Block, L. P., Double layers, Tech. Rept. TRITA-EPP-75-10, Dept. Plasma Physics, Royal Inst. Technology, Stockholm, Sweden, 1975.

Boyd, J. S., Rocket measurements of precipitating electrons in a system of multiple auroral arcs, Doctoral Thesis, Univ. of Alaska, Fairbanks, 1973.

Brown, N. B., T. N. Davis, T. J. Hallinan and H. C. Stenbaek-Nielsen, Altitude of pulsating aurora determined by a new instrumental technique, (submitted to Geophys. Res. Letters, 1976).

Buneman, O., R. H. Levy and L. Linson, The stability of crossed-field electron beams, J. Appl. Phys., 37, 3203-3222, 1966.

Carlqvist, P. and R. Boström, Space-charge regions above the aurora, J. Geophys. Res., 75, 7140-7145, 1970.

Carlqvist, P., On the formation of double layers in plasmas, Cosmic Electrodynamics, 3, 377-388, 1972.

Casserly, P. T., Jr. and P. A. Cloutier, Rocket-based magnetic observations of auroral Birkeland currents in association with a structured auroral arc, J. Geophys. Res., 80, 2165-2168, 1975.

Cloutier, P. A., H. R. Anderson, R. J. Park, R. R. Vondrak, R. J. Spiger and B. R. Sandel, Detection of geomagnetically-aligned currents associated with an auroral arc, J. Geophys. Res., 75, 2595-2600, 1970.

Cloutier, P. A., B. R. Sandel, H. R. Anderson, P. M. Pazich and R. J. Spiger, Measurement of auroral Birkeland currents and energetic particle fluxes, J. Geophys. Res., 78, 640-647, 1973.

Cutler, C. C., Instability in hollow and strip electron beams, J. Appl. Phys., 27, 1028-1029, 1956.

Dattner, A., Current-induced instabilities of a mercury jet, Arkiv För Fysik, 21, 7o-80, 1962.

Davis, T. N., An investigation of the morphology of the auroral displays of 1957-1958, Geophysical Inst. Rept. UAG-R117, Univ. of Alaska, Fairbanks, 1961.

Davis, T. N., The morphology of the auroral displays of 1957-1958: Part II: Detailed analyses of Alaska data and analyses of high latitude data, J. Geophys. Res., 67, 75-110, 1962.

Davis, T. N., Magnetospheric convection pattern inferred from magnetic disturbance and auroral motions, J. Geophys. Res., 76, 5978-5983, 1971.

Davis, T. N. and D. D. Wallis, Observations of ionospheric motions using barium ion clouds, Space Res., 12, 935-949, 1972.

Davis, T. N., Scientific design of a manned aurora and magnetosphere observatory system for the Shuttle program, Final Rept. on NASA Contract NAS 9-12649, Vol. I, 1973.

Doupnik, J. R., P. M. Banks, M. J. Baron, C. L. Rino and J. Petriceks, Direct measurement of plasma drift velocities at high magnetic latitudes, J. Geophys. Res., 77, 4268-4271, 1972.

Fairfield, D. H., Average magnetic field configuration of the outer magnetosphere, J. Geophys. Res., 73, 7329-7338, 1968.

Gartlein, C. W., Visual observation of the aurora, Annals Geophys., 15, 31-38, 1959.

Gould, R. W., Plasma Physics, (Ed. by F. H. Clauser), Addison-Wesley, Reading, Mass., pp. 98-100, 1960.

Gurnett, D. A. and L. A. Frank, Observed relationships between electric fields and auroral particle precipitation, J. Geophys. Res., 78, 145-170, 1973.

Hallinan, T. J., Small-scale auroral arc distortions, M.S. Thesis, Univ. of Alaska, Fairbanks, 1970.

Hallinan, T. J. and T. N. Davis, Small-scale auroral arc distortions, Planet. Space Sci., 18, 1735-1744, 1970.

Hallinan, T. J., T. N. Davis and H. F. Webster, Auroral spirals: A consequence of field-aligned currents, Geophysical Inst. Rept. UAG-R221, Univ. of Alaska, Fairbanks, 1972.

Hasegawa, A., Theory of auroral bands, Phys. Res. Lett., 24, 1162-1165, 1970.

Hays, P. B. and R. G. Roble, Direct observations of thermospheric winds during geomagnetic storms, J. Geophys. Res., 76, 5316-5321, 1971.

Heppner, J. P., A study of relationships between the aurora borealis and the geomagnetic disturbances caused by electric currents in the ionosphere, Doctoral Thesis, California Inst. of Technology, Pasadena, 1954.

Heppner, J. P., Electric field variations during substorms: OGO-6 measurements, Planet. Space Sci, 20, 1475-1498, 1972.

Johnstone, A. D. and T. N. Davis, Low altitude acceleration of auroral electrons during breakup observed by a mother-daughter rocket, J. Geophys. Res., 79, 1416-1425, 1974.

Joyce G. and C. Montgomery, Negative temperature states for the two-dimensional guiding-centre plasma, J. Plasma Phys., 10, 107-121, 1973.

Kan, J. R., Energization of auroral electrons by electrostatic shock waves, J. Geophys. Res., 80, 2089-2095, 1975.

Kern, J. W. and E. H. Vestine, Theory of auroral morphology, J. Geophys. Res., 66, 713-723, 1961.

Kim, J. S. and R. A. Volkman, Thickness of zenithal auroral arc over Fort Churchill, Canada, J. Geophys. Res., 68, 3187-3190, 1963.

Kintner, P. M. and L. J. Cahill, Jr., Current system in an auroral substorm, J. Geophys. Res., 79, 4326-4330, 1974.

Kyhl, R. L. and H. F. Webster, Breakup of hollow cylindrical electron beams, IRE Trans. Electron Devices, 3, 172-183, 1956.

Levy, R. H. and R. W. Hockney, Computer experiments on low density crossed-field electron beams, Phys. Fluids, 11, 766-771, 1968.

Maggs, J. E. and T. N. Davis, Measurements of the thickness of auroral structures, Planet. Space Sci., 16, 205-209, 1968.

Mozer, F. S. and R. Serlin, Magnetospheric electric field measurements with balloons, J. Geophys. Res., 74, 4739-4754, 1969.

Murty, G. S., Instability of a conducting fluid cylinder in the presence of an axial current, a longitudinal magnetic field and a coaxial conducting cylinder, Arkiv För Fysik, 19, 483-498, 1961a.

Murty, G. S., Instability of a conducting fluid slab carrying uniform current in the presence of a homogeneous magnetic field, Arkiv För Fysik, 19, 499-510, 1961b.

Oguti, T., Rotational deformations and related drift motions of auroral arcs, J. Geophys. Res., 79, 3861-3865, 1974.

Pierce, J. R., Instability of hollow beams, IRE Trans. Electron Devices, 3, 183-189, 1956.

Snyder, A. L., S.-I. Akasofu and T. N. Davis, Auroral substorms observed from above in the polar region by a satellite, J. Geophys. Res., 79, 1393-1402, 1974.

Störmer, C., The Polar Aurora, Oxford Univ. Press, Oxford, 1955.

Sugiura, M., Identifications of the polar cap boundary and the auroral belt in the high-altitude magnetosphere: A model for field-aligned currents, J. Geophys. Res., 80, 2057-2068, 1975.

Swift, D. W., On the formation of auroral arcs and acceleration of auroral electrons, J. Geophys. Res., 80, 2096-2108, 1975.

Swift, D. W., H. C. Stenbaek-Nielsen and T. J. Hallinan, An equipotential model for auroral arcs (accepted by J. Geophys. Res., 1975).

Webster, H. F., Structure in magnetically confined electron beams, J. Appl. Phys., 28, 1395-1397, 1957.

Webster, H. F. and T. J. Hallinan, Instabilities in charge sheets and current sheets and their possible occurrence in the aurora, Radio Science, 8, 475-482, 1973.

Wescott, E. M., J. D. Stolarik and J. P. Heppner, Electric fields in the vicinity of auroral forms from motions of barium vapor releases, J. Geophys. Res., 74, 3469-3487, 1969.

Wescott, E. M., H. C. Stenbaek-Nielsen, T. N. Davis, W. B. Murcray, H. M. Peek and P. J. Bottoms, The L = 6.6 OOSIK barium plasma injection experiment and magnetic storm of March 7, 1972, J. Geophys. Res., 80, 951-967, 1975a.

Wescott, E. M., H. C. Stenbaek-Nielsen, T. J. Hallinan, T. N. Davis and H. M. Peek, The SKYLAB barium plasma injection experiments, II: Evidence for a double layer (submitted to J. Geophys. Res., 1975b).

Yasuhara, F., Y. Kamide and S.-I. Akasofu, Field-aligned and ionospheric currents, Planet. Space Sci., 23, 1355-1368, 1975.

Zmuda, A. J. and J. C. Armstrong, The diurnal flow pattern of field-aligned currents, J. Geophys. Res., 79, 4611, 1974.

Figure 1 Line drawings of the cross sections of auroral arcs illustrate the three major rotational distortions; spirals, curls and folds. The spirals and folds are clockwise and the curls are counterclockwise.

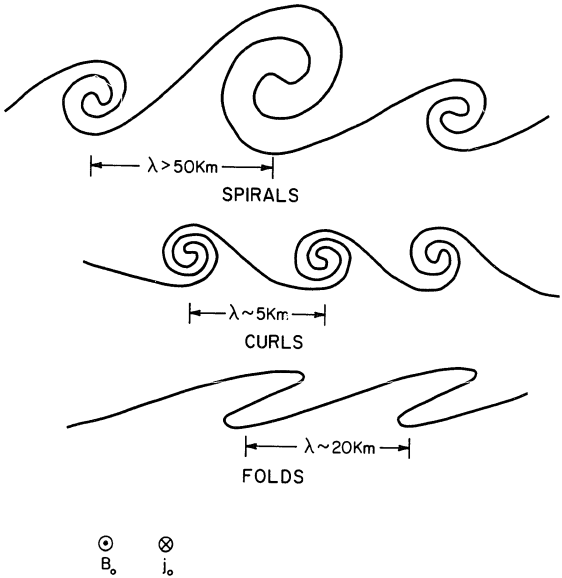

Figure 2 DMSP Satellite No. 6530 scanner images of spirals seen from above in the Northern Hemisphere (parallel to $\vec{B}$). The images are oriented with the direction toward the sun at top. Numbers refer to pass numbers, and listed times are approximately UT time the satellite passes over the aurora shown: Pass 1165, 0503 on 30 January 1973; Pass 403, 1548 on 7 December 1972; Pass 1304, 0743 on 9 February 1973; Pass 881, 0957 on 10 January 1973.

1165

403

1304

881

Figure 3 Same as Fig. 1 but showing examples of spirals with less symmetry. Pass 882, 140 on 10 January 1973; Pass 889, 2330 on 10 January 1973; Pass 926, 1419 on 13 January 1973; Pass 417, 1443 on 8 December 1972.

882

889

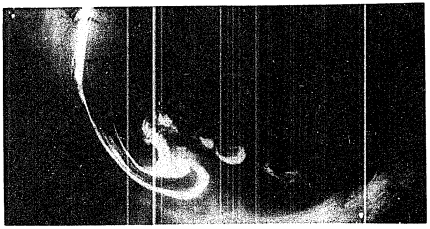

926

417

Figure 4 All-sky camera photographs from College and Fort Yukon, Alaska showing spirals seen from below (antiparallel to $\vec{B}$). Relatively small spirals overhead (A) are more easily recognized than large spirals (B and D) or spirals near the horizon (C).

A

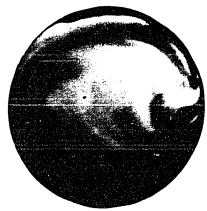

B

C

D

Figure 5 The distribution of spiral (minimum) diameters counting each spiral as one sample. The plot with shading represents spiral streets using the average minimum diameters of the spirals in each street.

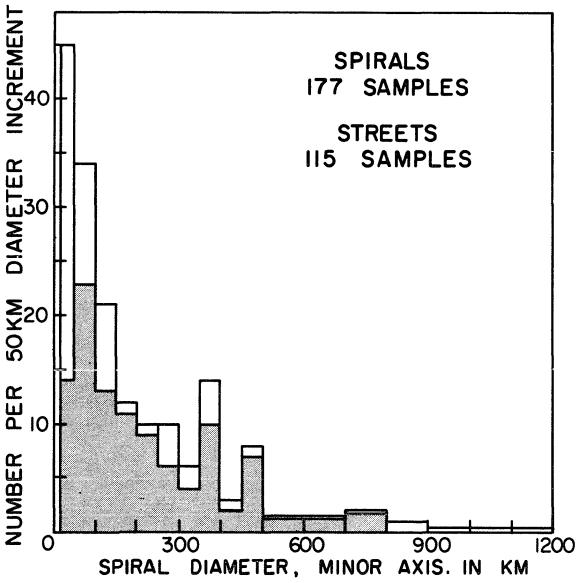

Figure 6 The distribution of the ratio of maximum to minimum spiral diameters; the median value is 1.7.

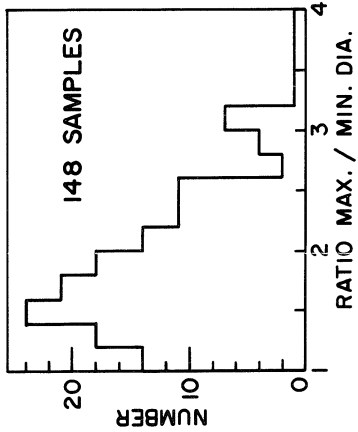

Figure 7 The occurrence distribution for ratios of λ/D where λ is the spacing between adjacent spiral centers and D is the average of the minimum diameters of the two spirals.

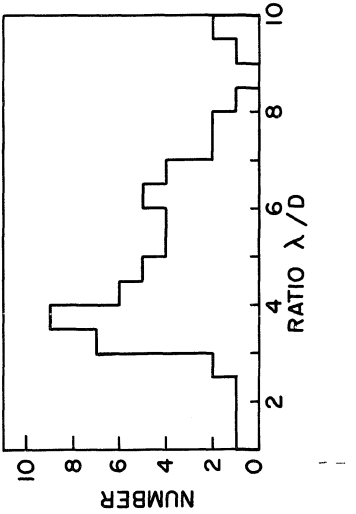

Figure 8 This schematic diagram shows the appropriate locations of spiral forms in local geomagnetic time relative to the location of the equatorward boundary of the diffuse aurora. The numbers near each bar refer to the DMSP satellite pass number; the bars are aligned along the major axis of the spirals. The latitudes have been normalized to a particular equatorward boundary at latitude 65^{o} in the midnight meridian.

Figure 9 Number of spirals observed as a function of local time at Barrow, Alaska (solid) and College, Alaska (dashed). This plot is the sum of twelve nights of simultaneous observations made in January, 1958.

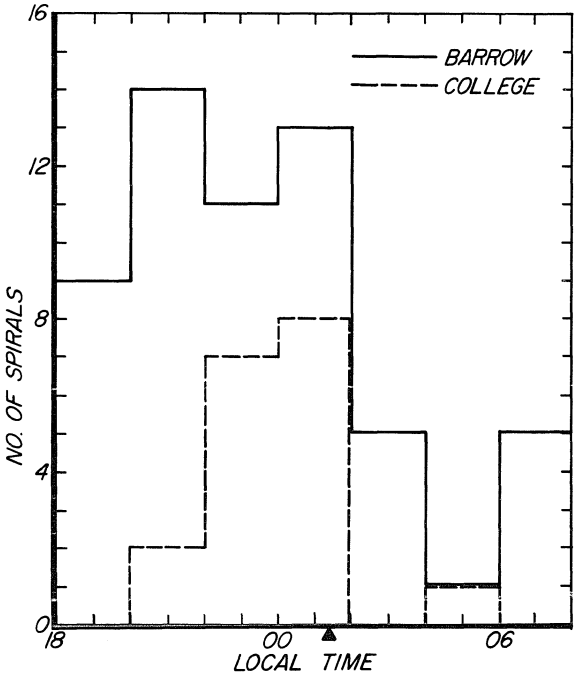

Figure 10 Photograph pairs showing the occurrence of counterclockwise curls within clockwise spirals. On the left are television pictures (1/8 sec exposure) with a horizontal field of view of approximately 35^{o}. On the right are the corresponding all-sky photographs (4 sec exposure). The rectangles in the all-sky photographs indicate the approximate coverage of the TV images.

Figure 11 A slab of current, of thickness 2a, is aligned parallel to a magnetic field B_o. Figure 1 shows the orientation of the slab and the direction of the current (j_o) and of the magnetic field (B_o).

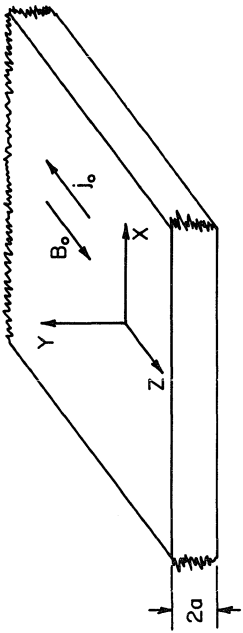

Figure 12 This illustration of the ripple distortion in a current sheet corresponds to the long-wavelength limit. The distortion implies a perturbation current density along z as shown. The small arrows indicate the direction of the x-y component of the magnetic field. Note the points of accumulation at $y = a$, $x = \frac{3\pi}{4}$ and at $y = -a$, $x = \frac{\pi}{4}$.

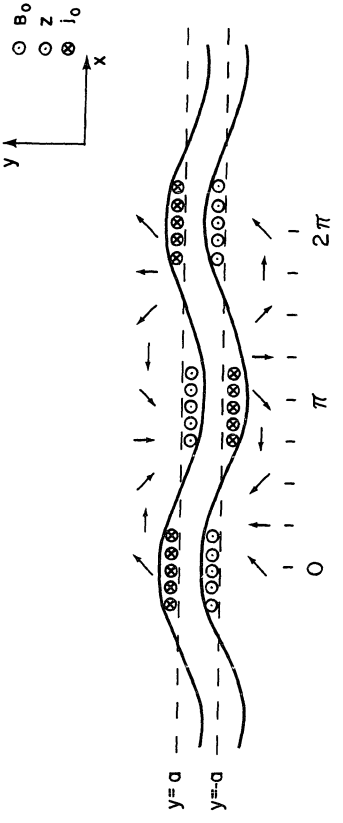

Figure 13 In the linear analysis the current sheet distortion consists of sine waves on the two boundaries. The phase angle (Kx_o) between the two surface waves in Fig. 2 is 0.35π and the wavelength to thickness ratio ($\lambda/2a$) is 7.9. These values correspond to the fastest growing mode. There is an accumulation of field lines and of current in the regions near x_1 and x_2. The distortion of the current sheet is clockwise with respect to these values of x.

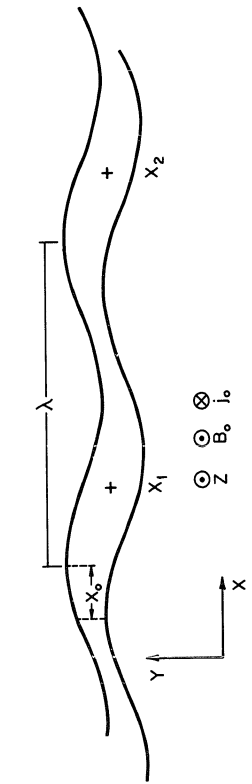

Figure 14 In Fig. 14, the quantity $i\beta B_o/\mu_o j_o$, which is proportional to the growth rate, is plotted as a function of the dimensionless number Ka. The wavelength to thickness ratio ($\lambda/2a$) is shown as a separate scale. The quantity Kx_o/π, which is a measure of the phase angle between the two surface distortions, is also plotted. The largest growth occurs for $Kx_o = 0.35\pi$ and $\lambda/2a = 7.9$. This leads to spirals. Larger values of $\lambda/2a$ correspond to smaller phase angles and hence result in folds.

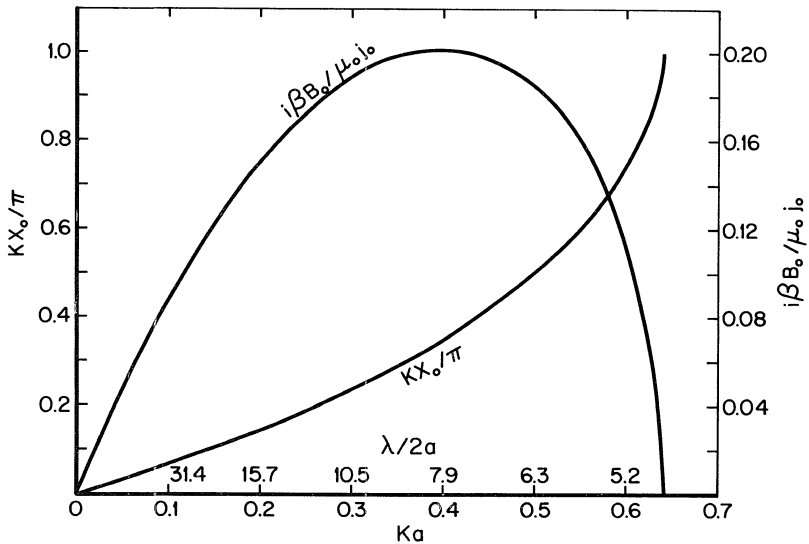

Figure 15 This figure is a schematic illustration of the development of a spiral array. An initial local current enhancement ($x = 0$ in part a) results in a fold (b) and further enhancement and distortion in (c). In (d) a spiral has formed and a new ripple is beginning to appear some distance (λ) to the right of the initial disturbance.

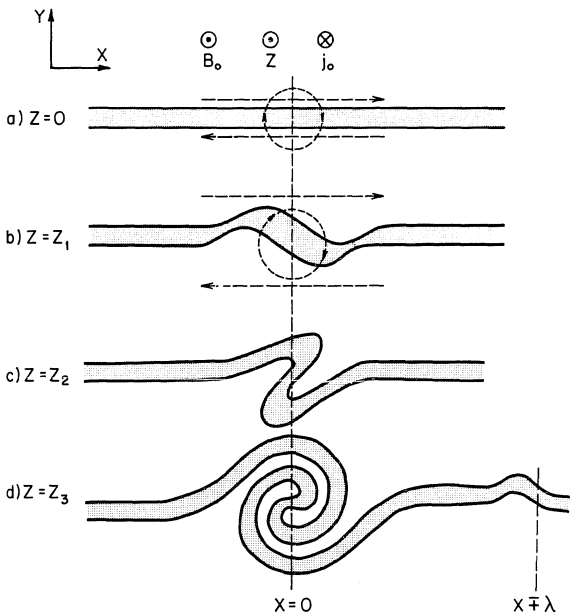

Figure 16 (After Homann, 1936) Streak lines in the wake behind a circular cylinder in a stream of oil illustrate the form which should be assumed by a balanced pair of oppositely-directed Birkeland sheet currents.

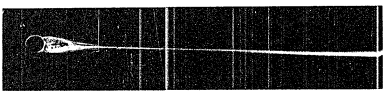

$R = 32$

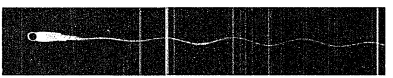

$R = 55$

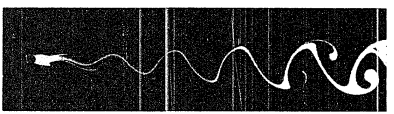

$R = 65$

$R = 73$

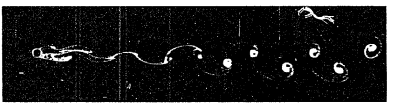

$R = 102$

$R = 161$